Article

Closing the Gap Between Experiment and Theory: Reactive Scattering of HCl from Au(111)

Published as part of The Journal of Physical Chemistry virtual special issue "Machine Learning in Physical Chemistry".

Nick Gerrits,* Jan Geweke, Egidius W. F. Smeets, Johannes Voss, Alec M. Wodtke, and Geert-Jan Kroes*

Read Online

ACCESS | Metrics & More | Article Recommendations | Supporting Information

ABSTRACT: Accurate simulation of molecules reacting on metal surfaces, which can help in improving heterogeneous catalysts, remains out of reach for several reactions. For example, a large disagreement between theory and experiment for HCl reacting on Au(111) still remains, despite many efforts. In this work, the dissociative chemisorption of HCl on Au(111) is investigated with a recently developed MGGA density functional (MS-RPBEl) and a high-dimensional neural network potential. Additionally, previous experimental sticking probabilities are re-examined. A considerably improved agreement between experiment and theory is obtained, although theory still overestimates experimental sticking probabilities by a factor of 2−7 at the highest incidence energy. Computed and measured vibrational transition probabilities are also in improved agreement. Several dynamical effects such as angular steering and energy transfer from the molecule to the surface are found to play an important role.
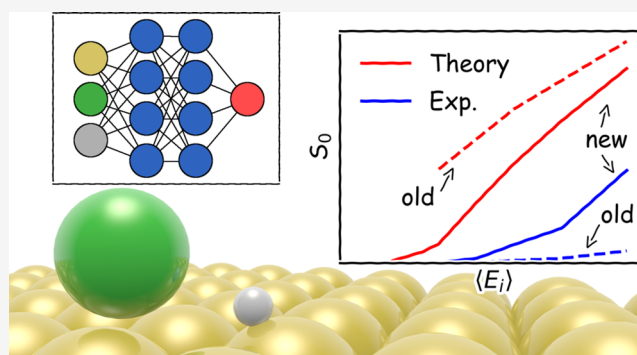
1. INTRODUCTION

Accurate first-principles simulation of the reaction of molecules on metal surfaces is of vital importance to understanding heterogeneous catalysis. Such simulations are continuously subject to improvements. For example, the development of high-dimensional neural network potentials (HD-NNP) allows molecular dynamics (MD) calculations on sticking while fully including the movement of surface atoms with computational costs orders of magnitude lower than those of ab initio molecular dynamics (AIMD).[1−5] Developments in density functional (DF) design[6−14] and wave function theory with DFT embedding[15,16] have led to an increasing number of surface reactions being described accurately. Furthermore, including the dissipative effect of electron−hole pair (ehp) excitations has enabled several accurate simulations that hitherto were impossible.[17−22] Nevertheless, many molecule−surface scattering processes[23] and reactions[5,24−27] exist for which accurate simulations remain elusive.

One molecule−surface reaction of particular interest is the dissociative chemisorption of HCl on Au(111). Although a large body of both theoretical and experimental work has shrunk the gap between theory and experiment,[2,27−37] quantitative agreement between the two is still out of reach. Dynamics calculations based on DFT potentials or forces have consistently overestimated experimental sticking probabilities

by more than an order of magnitude.[2,27,35,37] Throughout the years, development in theory often resulted in a lowering of the reactivity of HCl + Au(111): Going from a relatively attractive DF like PBE[38] or PW91[39] toward a repulsive DF like RPBE[40] lowers the initial sticking probability.[2,35,37] Including van der Waals correlation into the DF lowers the sticking probability even further.[27] Performing the MD with quasi-classical trajectories (QCT) or quantum dynamics (QD) appears to have little effect on the sticking probability.[37] Switching from a frozen to a mobile thermal surface is observed to lower the sticking probability, albeit only marginally.[2,27,35] Finally, treating the ehp excitations with the local density friction approximation (LDFA)[41] likewise has a small effect on the sticking probability.[2,27,35] Even so, in the most recent calculations theory still overestimated the sticking probability by more than an order of magnitude.[2,27]

Not only the sticking probability is subject of debate from a theoretical point of view, the vibrationally (in)elastic scattering

of HCl on Au(111) seems to be described inaccurately as well: No matter which model and method was employed, vibrational transition probabilities are systematically overestimated by theory. For example, enabling ehp excitation within the LDFA decreases transition probabilities by only a small amount.[2] Furthermore, since typically the QCT method is employed, the rovibrational states are not quantized during MD. Therefore, final rovibrational states need to be binned in order to obtain quantized rovibrational state populations. Although it is observed that Gaussian binning lowers the excitation probabilities compared to histogram binning, it remains to be seen what kind of binning method is the most appropriate one. For example, for H_2 + Pd(111) a single energy based Gaussian binning method, where also the diffraction quantum numbers are binned, performs comparatively well.[42] However, violation of Bohr's quantization does not present a problem as many rovibrational states are available for HCl + Au(111), and thus histogram binning should perform accurately as well.[43] An adiabatic correction was also employed for H_2 + Pd(111),[42,44] but for HCl + Au(111) such a correction would not make sense since many adiabatic paths are possible.[44] Finally, for elevated surface temperatures it is necessary to take into account surface atom motion.[2,27]

The transition and sticking probabilities measured by experiment are also subject to uncertainty.[27,32,34,35] An error was found in an initial report of $\nu = 0 \rightarrow \nu = 1$ inelastic scattering probabilities.[45] Revised probabilities are however now available with small uncertainty.[32] As will become clear, it is also necessary to reinvestigate the experimental sticking probabilities, of which accurate measurement poses considerable challenges. For this reason, experimental results on sticking from ref 34 are also re-examined here in the hope of more accurately characterizing the uncertainty of the measured sticking probabilities, thereby better clarifying the true magnitude of the discrepancy between experiment and theory.

As discussed above, many improvements have been made by theory and experiment for the description of the sticking and vibrational transition probabilities of HCl on Au(111). Nevertheless, the current state of affairs remains unsatisfactory. Therefore, in this work we focus on improving the employed DF in the hope of thereby improving the aforementioned observables in our simulations. Recently, a meta generalized gradient approximation (MGGA) DF has been developed, the "made simple" RPBE-like (MS-RPBEl) DF, which can describe both the molecule and the surface accurately, as well as the interaction between the two.[14] The MS-RPBEl DF yields chemically accurate (errors smaller than 1 kcal/mol or 4.2 kJ/mol) sticking probabilities for H_2 + Cu(111) and almost chemically accurate results for H_2 + Ag(111). Interestingly, for H_2 + Cu(111) the MS-RPBEl DF outperforms even state-of-the-art MGGA DFs like the revTPSS DF[46] by a large margin.[14] The MS-RPBEl DF is able to describe both the metallic and molecular orbital regimes by relying on a switching function that depends on the kinetic energy density. The overall functional form is derived from the RPBE functional.[40] To limit the self-interaction error (SIE) in the molecular orbital regime, which is fundamental to DFT,[47] the hydrogen atom is considered as the extreme case where any amount of electronic interaction constitutes an SIE. The analytical solution to the H charge density and SIE is used to parametrize the single-electron limit of the meta-GGA, and correctly reproducing this limit has been shown to improve surface reaction energetics also for multielectron adsorbates.[14,48] For the metallic density

regime on the other hand, the low order gradient expansion of the exchange energy of the homogeneous electron gas is reproduced, ensuring good description of lattice constants and elastic properties. Since the MS-RPBEl DF has provided promising initial results and contains fundamental advantages that might be of importance for the reaction of HCl on Au(111), we will test this functional in this work. Additionally, in order to be able to perform MD calculations with surface atom motion modeled explicitly an HD-NNP will be employed, allowing observables with low probability to be obtained with relatively small statistical errors.

To summarize, in this work the newly developed MS-RPBEl DF is tested for vibrationally inelastic scattering and sticking of HCl on Au(111). Additionally, previous experimental sticking probabilities[34] are revisited. As we will show, a considerably improved agreement between theory and experiment is obtained, although discrepancies still remain. Furthermore, several aspects of the reaction dynamics, such as the influence of surface atom motion, energy transfer, vibrational efficacies, the bobsled effect, and site specificity, are discussed as well.

2. METHOD

2.1. Theory. For the electronic structure (density functional theory, DFT) calculations the Vienna ab-initio simulation package (VASP version 5.4.4)[49−53] is used. We use the "made simple" revised Perdew, Burke and Ernzerhof (MS-RPBEl) meta-GGA exchange-correlation functional, which has been introduced in ref 14. The design of this functional is based on the MS philosophy underlying earlier functionals of this kind.[54,55] The first Brillouin zone is sampled by a Γ-centered 8 × 8 × 1 k-point grid and the plane wave kinetic energy cutoff is 600 eV. Moreover, the core electrons have been represented with the projector augmented wave (PAW) method.[53,56] The surface is modeled using a 4 layer (3 × 3) supercell, where the top three layers have been relaxed in the Z direction and a vacuum distance of 15 Å is used between the slabs. The bulk optimized lattice constant is 4.092 Å, which is in excellent agreement with the experimental value of 4.078 Å.[57] Furthermore, the outward interlayer relaxation of the top two layers is 3.0%, which is in reasonable agreement with the experimental value of 1.5%.[58] Note that the interlayer relaxation is not well converged, but this does affect the results presented in this work considerably (see Supporting Information). In order to simulate a surface temperature of 170 K, the lattice constant is multiplied with a thermal expansion coefficient of 1.0014, as has been done in refs 35 and 27. First order Methfessel−Paxton smearing[59] with a width parameter of 0.2 eV has been employed. The aforementioned computational setup is confirmed to yield a barrier height that is converged with respect to the input parameters to within chemical accuracy (1 kcal/mol, or 4.2 kJ/mol), as shown in the Supporting Information.

The transition state is obtained with the dimer method[60−63] as implemented in the VASP Transition State Tools package (VTST), and is confirmed to be a first order saddle point. Forces along the degrees of freedom are converged to within 5 meV/Å, where only HCl is relaxed in all its six degrees of freedom and the surface atoms are kept fixed in their ideal positions.

The initial conditions of the HCl molecules are generated in the same way as in ref 35, which we will summarize here. The center of mass (COM) velocity v of HCl is given by the flux weighted probability distribution

$$f(v; T_N) \, dv = Av^3 \exp^{-(v-v_0)^2/a^2} dv \tag{1}$$

where T_N is the nozzle temperature, A is a normalization constant, $v_0 = \sqrt{2E_0/M_{HCl}}$ is the stream velocity, and a is the width of the distribution. The rovibrational state population $F_{v,j}$ is given by

$$F_{v,j}(T_N) = \frac{2j+1}{Z(T_N)} \exp^{-(E_{v,0}-E_{0,0})/k_B T_{vib}} \exp^{-(E_{v,j}-E_{v,0})/k_B T_{rot}} \tag{2}$$

where $Z(T_N)$ is the partition function, $T_{vib} = T_N$, and $T_{rot} = -181.1 + 0.648 T_N$. All incidence conditions are normal to the surface (i.e., $v_X = v_Y = 0$), unless noted otherwise. The beam parameters describing the velocity and rovibrational state distributions are obtained from refs 29 and 34 and are summarized in Tables 1 and 2. In general, the parameters of

Table 1. Beam Parameters from Reference 29 That Describe the Simulated HCl Velocity Distributions[a]

T_N (K)	$\langle E_i \rangle$ (kJ/mol)	E_0 (kJ/mol)	v_0 (m/s)	α (m/s)
300	27	27	1210	52
300	31	31	1297	60
300	43	43	1542	67
300	50	51	1665	48
300	75	75	2031	114
300	94	94	2276	98
300	122	123	2601	81

[a]The stream energy E_0, stream velocity v_0, and width parameter α are determined through time-of-flight measurements. The nozzle temperature is assumed to be room temperature.

Table 2. Same as Table 1 but from Reference 34

T_N (K)	$\langle E_i \rangle$ (kJ/mol)	E_0 (kJ/mol)	v_0 (m/s)	α (m/s)
296	91	90	2219	158
400	114	110	2456	245
500	124	120	2562	207
620	150	144	2808	292
740	174	167	3026	323
910	205	196	3278	364
1060	247	238	3616	371

Tables 1 and 2 are used when investigating vibrational transition and sticking probabilities (and their related observables), respectively. When the parameters of both tables are employed due to the need of describing a large incidence energy range, Table 1 is used up to 94 kJ/mol and Table 2 is used from 114 kJ/mol. The initial thermal distortions and velocities of the surface atoms are sampled from 50 slabs that were first equilibrated for 1 ps and simulated for an additional 1 ps, using a time step of 1 fs. Only configurations of the final ps in the simulations were sampled in the simulations of the collision dynamics, yielding 50 000 initial surface configurations. Additional details about the surface atom motion sampling procedure can be found in ref 64.

Molecular dynamics calculations have been performed using LAMMPS.[65,66] All trajectories are propagated up to 3 ps using a time step of 0.4 fs, or until HCl either scattered or reacted. The time step size is deemed adequate as the energy conservation error is quite good for the vibrational ground state (1−2 meV) and reasonably good for the $v = 2$ vibrationally excited HCl 5−10 meV during the trajectories.

A smaller time step would decrease the energy conservation error, but we have checked that the choice of time step size does not affect the reaction and vibrational transition probabilities. HCl is considered reacted when the bond length becomes 3 Å or longer, and is considered scattered when the distance between the COM of HCl and the surface becomes larger than 7.5 Å and the velocity vector is pointing away from the surface. If the molecule neither reacted nor scattered within 3 ps, the molecule is considered to be trapped. The sticking probability is then defined as

$$S_0 = \frac{N_{reacted} + N_{trapped}}{N_{reacted} + N_{trapped} + N_{scattered}} \tag{3}$$

For each sticking data point 10 000 trajectories have been simulated. Where 10 000 trajectories yield too large statistical errors in the desired observables, e.g., when scattering to specific rovibrational states was investigated, 100 000 trajectories have been run. The vibrational and rotational action (x and J) of scattering trajectories are given by

$$x = \frac{1}{2\pi} \oint p_r \, dr - \frac{1}{2} = \frac{1}{2\pi} \int_0^\tau p_r \dot{r} \, d\tau - \frac{1}{2} \tag{4}$$

$$J = -\frac{1}{2} + \sqrt{\frac{1}{4} + L_f^2} \tag{5}$$

and

$$L_f = p_\theta^2 + \frac{p_\phi^2}{\sin^2(\theta)} \tag{6}$$

where r is the HCl bond length and p_r its conjugate momentum, and p_θ and p_ϕ are the momenta conjugate to the θ and ϕ angles of HCl, which will be discussed later. In the vibrational action integral (eq 4), the vibrational momentum p_r is evaluated over a single vibrational period τ. Furthermore, the concomitant quantum number is obtained by rounding the action to the nearest integer (standard or histogram binning).

Previous studies show that ehp excitation, when modeled with electronic friction at the local density friction approximation level, has only a marginal effect on the sticking and the vibrationally (in)elastic scattering of HCl on Au(111).[2,27,35] Moreover, since, as we will show even with an improved setup, a fairly large discrepancy persists between theory and experiment, in this work we neglect the effect of ehp excitation, and instead focus on the effect of the exchange-correlation functional.

To develop the HD-NNP we used the Behler−Parrinello approach.[67,68] In this approach, the total energy is constructed as a sum of atomic contributions that are dependent on their chemical local environment and are described by many-body atom-centered symmetry functions.[69] In total, 29 500 DFT calculations were performed, of which 90% were used to train and 10% to test the HD-NNP. The configurations that were used in the DFT calculations to generate the data set are summarized in Table 3. A total of 8500 configurations were generated that excluded surface atom motion (i.e., for the ideal frozen surface) and 21 000 configurations were generated including surface atom motion. Surface atom motion was included by displacing surface atoms according to a harmonic oscillator model, as described in ref 64. Z_{Cl} and r were sampled randomly in the ranges described in Table 3, and the other degrees of freedom of HCl (X_{Cl}, Y_{Cl}, θ, and ϕ) were also

Table 3. Parameters Used to Generate Configurations in the DFT Calculations to Generate the Training and Testing Data Set for the HD-NNP

surface atom motion	Z_{Cl} (Å)	r (Å)	N
no	2.5−8.0	1.0−1.6	6000
no	1.5−2.5	1.0−3.2	2500
yes	2.5−8.0	1.0−1.6	6000
yes	1.5−2.5	1.0−3.2	15000

sampled randomly, with the only constraint that $Z_H > 0.5$ Å. Finally, it was confirmed that the occurrence of extrapolation errors due to missing structures in the data set was sufficiently low that it had a negligible effect on the sticking probability. The RMSE of the energies and forces of the training data set is 1.0 and 2.3 kJ/mol/Å, respectively, which is well within chemical accuracy. Additional details regarding the fitting accuracy are provided in the Supporting Information. For the neural network, two hidden layers are used, each with 15 nodes. The training has been carried out using the RuNNer code.[70−72] The employed symmetry functions are described in ref 1, and the concomitant parameters have been obtained following the procedure of ref 73 and are provided in the Supporting Information.

2.2. Experiment. The experimental apparatus has been described in detail before[34,45] as were the methods to determine the initial sticking probabilities.[34] Thus, after briefly recalling the most important experimental details here, further on we will focus on the changes in data *analysis*.

Pulsed molecular beams of 4% HCl seeded in H_2 were directed at a Au(111) single-crystal (orientation accuracy better than 0.1°, purity 99.999%, MaTecK) with a surface temperature of $T_S = 170$ K held in an ultra-high vacuum chamber with base pressure ~2×10^{-10} Torr. A wide range of translational energies, $\langle E_i \rangle = 91-247$ kJ/mol, was obtained by mounting a ~ 20 mm long SiC tube to the front of the home-built, solenoid-based valve and resistively heating it to as high as $T_N = 1140$ K. We used resonance-enhanced multiphoton ionization to quantify the ro-vibrational population distributions which also varied with T_N according to eq 2. During exposure, the H_2 pressure rise in the UHV chamber was recorded with a mass spectrometer (SRS RGA-200) from which we could derive the dose of HCl molecules ϕ_{HCl} via the previously determined HCl/H_2 pressure ratio in the gas mix. After dosing, the chlorine coverage, Θ_{Cl}, was derived using an Auger electron spectrometer (Physical Electronics Φ15-255G) by measuring the ratio of the peak heights at 181 eV (Cl) and 239 eV (Au).

3. RESULTS

3.1. Experimental Sticking Probabilities. Initial sticking probabilities S_0 are determined from the dependency of the chlorine coverage Θ_{Cl} on the applied HCl dose ϕ_{HCl}, both of which have recently been reanalyzed. In general, the incident dose is calculated as

$$\phi_{HCl} = \frac{N_{H_2}}{A_{MB}} \times \frac{c_{HCl}}{c_{H_2}} \times f_e \times \frac{1}{N_{ML}} \qquad (7)$$

Here, N_{H_2} is the number of incident H_2 molecules, A_{MB} is the cross-sectional area of the incident molecular beam, c_{HCl} and c_{H_2} are the concentrations in the prepared gas mixture, and f_e is the correction factor for the hydrodynamic enrichment of the

heavier HCl molecules. Due to the higher mass of HCl relative to that of H_2, the concentration of HCl molecules in the center of the molecular beam is up to ten times higher in the UHV chamber than in the prepared gas mixture (see the Supporting Information of ref 34). Furthermore, N_{ML} is the areal number density of Cl atoms per monolayer (ML) on the unrecon-structed Au(111) surface (assuming one ML coverage corresponds to one Cl atom per every surface top layer Au atom). Compared to a previously published analysis,[34] its value was more accurately determined to be 1.39×10^{15} cm^{-2} ML^{-1} instead of 1×10^{15} cm^{-2} ML^{-1}, in accordance with values reported by Kastanas and Koel.[74]

The chlorine coverage resulting from a controlled HCl dose, Θ_{Cl}, is calculated from the atomic concentration of Cl on the surface, C_{Cl}, relative to the saturation coverage. This can be obtained from the Auger peak heights I_{Cl} and I_{Au} for Cl and Au, which can be combined to the peak-height ratio $P_r = I_{Cl}/I_{Au}$, and the corresponding Auger sensitivities S_{Au} and S_{Cl}:[34]

$$C_{Cl} = \frac{I_{Cl}}{S_{Cl}} \bigg/ \left(\frac{I_{Cl}}{S_{Cl}} + \frac{I_{Au}}{S_{Au}} \right) = \frac{P_r \times S_{Au}}{P_r \times S_{Au} + S_{Cl}} \qquad (8)$$

$$\Theta_{Cl} = \frac{C_{Cl}}{C_{Cl,sat.}} \qquad (9)$$

Re-evaluating the literature for the saturation value of P_r[75] and the element-specific Auger sensitivity factors[76] reveals the saturation value for the atomic concentration of Cl on Au(111) ($C_{Cl,sat.}$) to be 0.13 ML^{-1}, which is slightly lower than the one (0.2 ML^{-1}) used in the previous analysis.[34] As a result the new measured S_0 values presented here have, to a good approximation, increased by a factor 0.2/0.13 = 1.54. For this work, we have also considered the possible influence of diffusion of Cl atoms on the gold surface. This could dilute the chlorine concentration in the center of the surface spot which was hit by the molecular beam, resulting in a radial gradient of C_{Cl}.

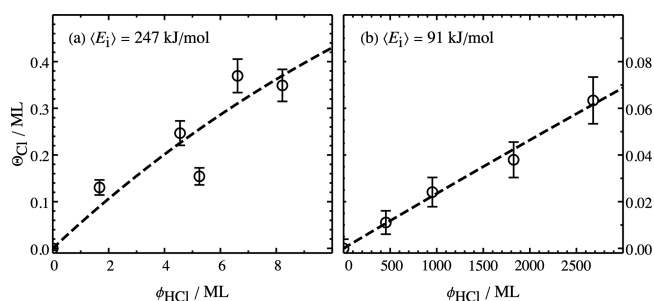Resulting coverage vs dose data is shown in Figure 1 for two representative conditions chosen to cover high and low

Figure 1. Representative plots of the Cl coverage Θ_{Cl} on the surface vs the applied dose ϕ_{HCl} for $\langle E_i \rangle = 247$ kJ/mol (a) and $\langle E_i \rangle = 91$ kJ/mol (b). Open symbols denote the data calculated according to eqs 7 and 9, the dashed lines show fits according to eq 10.

incidence energies. We note that parts a and b of Figure 1 are representative in the sense that they show the amount of scatter that may occur in the measurement of coverage vs HCl exposure, but not in the sense that the scatter is systematically higher at higher incidence energies. To obtain initial sticking probabilities, the data are fitted with a bounded growth model according to eq 10. Assuming an asymptotic saturation

coverage of $\Theta_{Cl} = 1$ ML, the only fit parameter is S_0, which corresponds to the initial slopes of the dashed lines in Figure 1.

$$\Theta_{Cl} = 1 - \exp(-S_0 \times \phi_{HCl}) \tag{10}$$

Two further systematic corrections to the data upon which the derivation of S_0 is based are needed. First, additional calibration experiments have shown that in comparison with an ion gauge, the mass spectrometer overestimated the H_2 partial pressure, which is integrated to obtain N_{H_2}, by a factor of $f_{IG} = 1.8$. That is, the dose determined with the mass spectrometer needs to be decreased by the same factor. Unfortunately, f_{IG} was determined with an ion gauge that itself was not calibrated against any known standard which limits the correction's accuracy.[106] Second, as reported in the Supporting Information of ref 34, the derived Cl-surface coverage exhibited a surface temperature dependence: for high T_S the resulting Θ_{Cl} was reduced. More specifically, the coverage derived at the lowest accessible temperature, $T_S = 80$ K, was a factor of $f_{T_S} = 1.4$ higher than that obtained at 170 K, the temperature used for the reactive dosing experiments. We attribute these differences to additional sticking of undissociated HCl by a physisorption interaction possible at 80 K but not at 170 K and to changes in the competitive kinetics for the associative desorption of H_2 and HCl with changes in surface temperature.

Despite the fact that the combined effect of these two corrections is not clear, the systematic direction of their influence on S_0 is; hence, lower and upper limits to the dissociative sticking probabilities can be derived. If both f_{IG} and f_{T_S} corrections are applied, we obtain an upper limit to the sticking probability. If both corrections are ignored, we obtain a lower limit. This is shown in Figure 2 for the sticking probability of HCl on Au(111) as a function of mean translational incidence energy. There, the two limits comprise all statistical and systematical uncertainties resulting from the experiments and the analysis. These also include the uncertainties from the fitting process due to the aforementioned scatter in the coverage vs HCl exposure data.

3.2. Potential Energy Surface. In Figure 3 the minimum barrier geometry obtained with the MS-RPBEl DF and the spherical coordinate system used throughout this work are depicted: The distance between the Cl atom and the surface Z_{Cl}, the HCl bond length r, and the polar and azimuthal angles of the HCl bond θ and ϕ with respect to the surface normal and lateral skewed vector u, respectively. The HCl bond is defined as the vector going from the Cl atom to the H atom. Furthermore, the lateral coordinates X and Y indicate the XY plane, where X and u are identical. The angle between the lateral skewed coordinates u and v is 60 deg. Since the interaction between HCl and the fcc and hcp sites is similar, they are also referred to as hollow sites throughout this work.

The minimum barrier geometries and heights computed with DFT using the MS-RPBEl, RPBE, RPBE-vdW-DF1 and SRP32-vdW-DF1 functionals are compared in Table 4. All barrier geometries are similar, except for the RPBE DF for which the COM is near the top2fcc site (i.e., the site midway between the top and fcc sites) and the HCl bond points toward the fcc site. The RPBE DF yields an earlier barrier ($r = 1.95$ Å) than the other DFs ($r \approx 2.2$ Å). Furthermore, RPBE yields for HCl a gas phase bond length of 1.27 Å, whereas the other DFs yield a bond length of 1.28−1.29 Å. The COM of the other barrier geometries is near the top site and the HCl
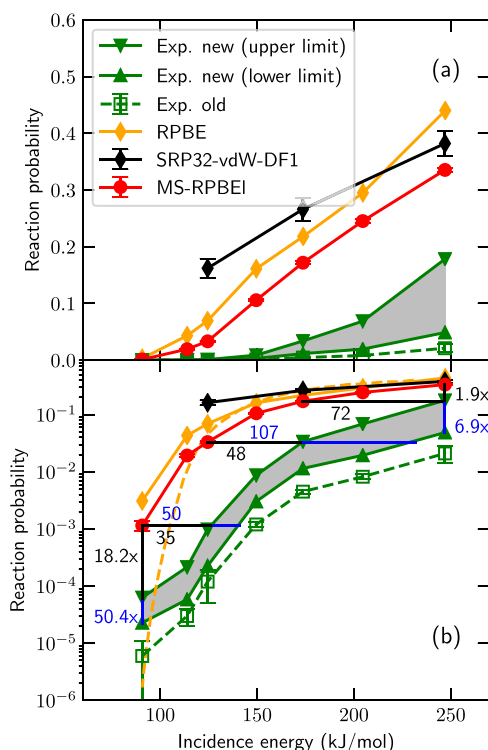

Figure 2. (a) Sticking probability of HCl on Au(111) for normal incidence and $T_S = 170$ K. The open green squares connected with a dashed line indicate the experimental results from ref 34, and the closed green triangles indicate the new experimental results, where the gray area indicates the area between the lower and upper limits. The theoretical results obtained with the SRP32-vdW-DF1,[27] RPBE,[2] and MS-RPBEl DFs are indicated by black diamonds, orange diamonds, and red circles, respectively. The error bars represent 68% confidence intervals. (b) Same as panel a, but using a logarithmic scale. The solid orange line with diamonds and the dashed orange line without diamonds indicate results for the RPBE DF employing QCT and QD, respectively. The horizontal (vertical) black (blue) lines indicate the difference between the computed and measured results for the newly determined upper (lower) limit.

bond points toward the bridge site. Several other GGA DFs incorporating the nonlocal van der Waals correlation functional of Dion and co-workers (vdW-DF1)[77] have been tried as well and yield similar geometries,[27] where only the barrier height is considerably affected.[27] Furthermore, the PBE functional yields a similar barrier geometry as RPBE but again different barrier heights are obtained.[27] Interestingly, the MS-RPBEl DF yields a similar geometry as the GGA-vdW-DF1 DFs, even though it is lacking van der Waals correlation and for this reason might be expected to yield results more similar to the (R)PBE DFs. Moreover, with the MS-RPBEl functional one of the highest barrier heights so far is obtained, where to the best of our knowledge with the DFs tested only with RPBE a higher barrier height was obtained.

The barrier geometries and heights obtained from the HD-NNP fit to the MS-RPBEl data at several high symmetry sites are provided in Table 5, where X_{Cl} and Y_{Cl} are fixed above the high symmetry sites. Note that the small differences between Tables 4 and 5 for the minimum barrier obtained with DFT is due to excluding or including the lattice expansion corresponding to $T_S = 170$ K, respectively. Moreover, the minimum barrier geometries and heights obtained with HD-NNP are in excellent agreement with DFT. The order of
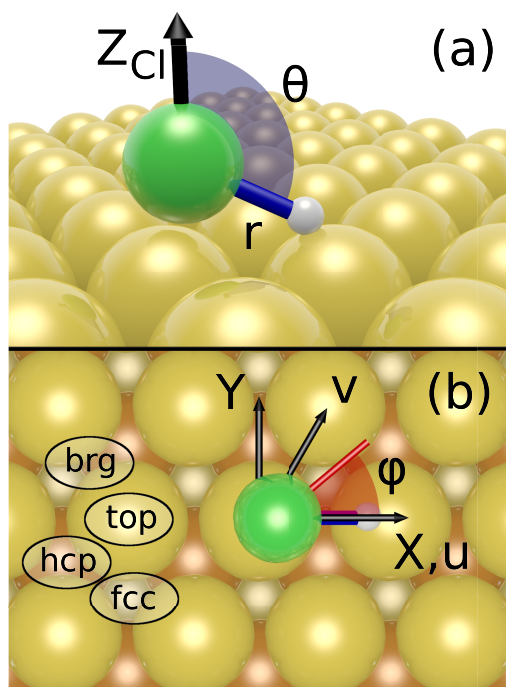
Figure 3. Minimum barrier geometry of HCl on Au(111) using the MS-RPBEl functional. The Cl atom is indicated in green, the H atom in white, and the Au atoms in gold, orange and gray (first, second, and third layer, respectively). The spherical coordinate system used throughout this work is depicted: (a) the distance between the Cl atom and the surface Z_{Cl}, the HCl bond length r, and the polar angle θ, which is defined by the vector pointing from Cl to H and the surface normal; and (b) the lateral coordinates X and Y, the lateral skewed coordinates u and v, and the azimuthal angle ϕ, which defines that projection of the Cl to H vector on the surface. The lateral coordinates may refer to Cl or the COM. Note that for ϕ not the value for the barrier is depicted but an arbitrary value. The top, bridge (brg), and hcp, and fcc hollow sites are indicated as well.

Elbow plots corresponding to the aforementioned site specific and global minimum barrier geometries are shown in Figure 4. The procedure for obtaining the minimum energy path (MEP) is described in the Supporting Information (see also Figure S7). In general, the barrier is late and high. Furthermore, most of the barriers seem to exhibit reasonable dynamical accessibility as the MEP typically does not make a sharp turn. However, the top site clearly is an exception as the MEP does not only make a sharp turn, but also goes up sharply in the Z_{Cl} coordinate after the turn, leading to low dynamical accessibility of the minimum barrier at the top site. Moreover, it is quite possible that HCl would not follow the MEP's turn at the top site at all, but rather would go down further along the Z_{Cl} coordinate. This would result in HCl hitting a large repulsive wall and subsequent scattering of the molecule, reducing the overall reactivity of the top site. In Figure 5 we also show the MEP as it is obtained in a more conventional way, performing a steepest descent from the top site minimum barrier. Figure 5b suggests that HCl would need to undergo a considerable reorientation in the θ angle going from the gas phase to the TS, which could reduce the dynamical availability of the top site TS even further as large dynamical steering in the θ angle is required. Also, since the MEP leading to the TS (gray circles) is different from the steepest descent away from the TS (white circles), it is possible that desorption would follow a different path than dissociative chemisorption.

Electronic (β) and mechanical (α) couplings of the minimum barrier of HCl on Au(111) computed using the MS-RPBEl functional are shown in Figure 6. The electronic coupling indicates the change in barrier height as a function of surface atom puckering, whereas mechanical coupling indicates the change in location, i.e., Z_{Cl}, as a function of surface atom puckering. The effect of puckering of the two top layer atoms nearest to the Cl and H atoms appears to be additive, i.e., the effect of the simultaneous puckering of the two multiple surface atoms nearest to Cl and H and the concomitant coupling parameters can be approximated by summing the contributions due to the puckering of the individual surface atoms. Furthermore, the surface atom near the H atom has a larger effect on the electronic coupling than the surface atom near the Cl atom, and vice versa for the mechanical coupling. The electronic coupling of HCl with the surface atom nearest to H is weaker by a factor 4.6 than that found in CH$_4$ + Ni(111) (112 kJ/mol/Å), while the mechanical coupling of HCl with the surface atom nearest to Cl is of similar magnitude as that in CH$_4$ + Ni(111).[78]

3.3. Sticking Probabilities Predicted by Theory. In Figure 2a the sticking probabilities computed for normal incidence and T_S = 170 K with the MS-RPBEl functional are compared to both the old and new experimental sticking probabilities and are found to be in improved agreement. Nevertheless, a large discrepancy still remains, where the

the barrier heights is global < bridge < top < hollow. It is also expected that the hollow site barrier is the highest on the basis of the location of the minimum barrier, which is located near the top site and for which the Cl−H bond points toward the bridge site. Furthermore, the geometry at the hollow sites is similar to the minimum barrier geometry, where the HCl also points toward a top site (see Figure 3). The bridge site geometry is also similar to the minimum barrier, with the only differences being that it is an earlier barrier (i.e., a smaller r value) and the HCl bond is oriented toward the hcp site. Finally, the top site geometry is different in location, bond length and polar orientation (θ) of the HCl bond compared to the minimum barrier, while the only similarity between the two being the azimuthal orientation (ϕ).

Table 4. Minimum Barrier Geometry and Height of HCl on Au(111) Obtained with DFT Using Different Functionals for T_S = 0 K[a]

functional	Z_{Cl} (Å)	r (Å)	θ (deg)	ϕ (deg)	COM$_u$ [L]	COM$_v$ [L]	E_b (kJ/mol)
MS-RPBEl	2.43	2.18	115	1	0.145	0.023	100.6
RPBE[35]	2.44	1.95	135	30	0.328	0.164	101.3
RPBE-vdW-DF1[27]	2.45	2.20	115	0	0.199	0.016	78.9
SRP32-vdW-DF1[27]	2.43	2.22	114	0	0.197	0.026	62.1

[a]The lateral skewed coordinates u and v of the center of mass (COM) are given in units of the surface lattice constant L.

**Table 5. Barrier Geometries and Heights of HCl on Au(111) on Different Sites Obtained from the HD-NNP Fit to the MS-RPBEl Data for T_S = 170 K[a]**

site	Z_{Cl} (Å)	r (Å)	θ (deg)	ϕ (deg)	COM_u [L]	COM_v [L]	E_b (kJ/mol)
global (DFT)	2.45	2.08	117	0	0.117	0.009	100.4
global	2.46	2.08	117	0	0.200	0.005	99.9
bridge	2.39	1.96	119	30	0.509	0.509	109.3
top	2.59	1.89	135	2	0.000	0.012	115.5
Fcc	2.42	2.20	113	90	0.322	0.356	128.0
Hcp	2.42	2.20	113	30	0.678	0.678	128.3

[a]The lattice expansion is included according to the surface temperature. The minimum barrier obtained directly from DFT is included as well. The lateral skewed coordinates u and v of the center of mass (COM) are given in units of the surface lattice constant L.
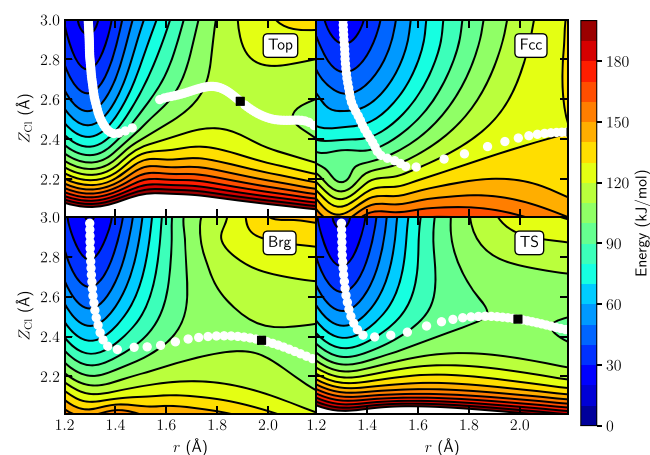
Figure 4. Elbow plots of HCl on Au(111) as a function of Z_{Cl} and r using the MS-RPBEl functional for the top, fcc, and bridge sites, and the minimum TS. All other degrees of freedom are relaxed. Black contour lines are drawn at an interval of 10 kJ/mol between 0 and 200 kJ/mol. The white circles indicate the MEP in reduced dimensionality and the black square indicates the highest point along the MEP. Note that the break along the MEP is an artifact caused by the procedure employed to obtain the MEP (see Figure S7).

Figure 6. Electronic (β) and mechanical (α) coupling at the minimum barrier of HCl on Au(111) using the MS-RPBEl functional. Variation of the barrier height E_b, and the distance of Cl to the surface Z_{Cl}, with the coordinate associated with the (simultaneous) motion(s) of the top layer surface atom(s) (Q) nearest to Cl, H, or both is indicated by the blue, red and orange circles, respectively. A positive value of Q indicates one atom or both atoms puckering out of the surface. The lines are linear regression fits to the data. The numbers in the plot indicate the electronic (β, kJ/mol/Å) and mechanical (α) coupling parameters, which are obtained from the slope of the linear regression fits.

overestimation is a factor 2 to 7 at the highest incidence energy (see Figure 2b). Sticking probabilities previously obtained with the SRP32-vdW-DF1 and RPBE functionals are included as well, and these are higher than those obtained with the MS-
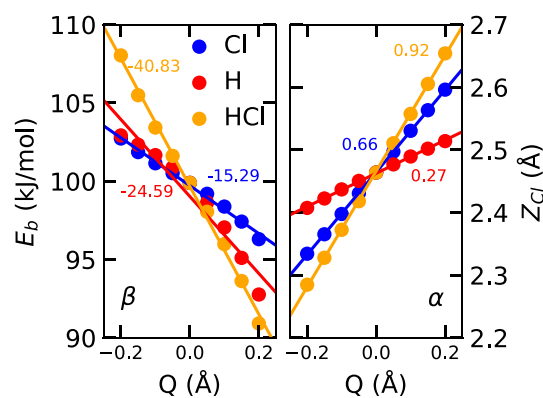
RPBEl DF. The QCT and QD results sticking probabilities obtained with the RPBE DF in ref 2 are compared in Figure 2b. For incidence energies well above the minimum barrier height the QCT and QD results are in good agreement,
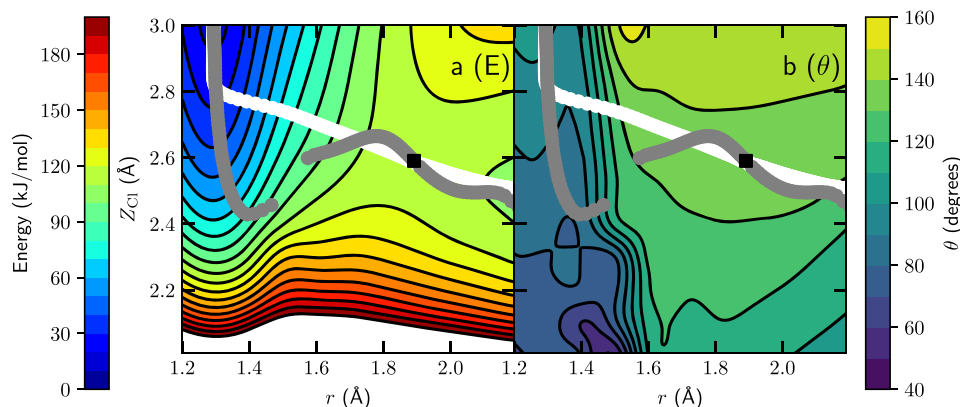

Figure 5. Elbow plots of HCl on Au(111) as a function of Z_{Cl} and r using the MS-RPBEl functional for the top site showing the energy (a, kJ/mol) and the θ angle (b, deg). All degrees of freedom other than Z_{Cl} and r are relaxed. Black contour lines are drawn at an interval of 10 kJ/mol between 0 and 200 kJ/mol (energy) or at an interval of 10° between 40° and 160° (θ). The gray circles indicate the MEP in reduced dimensionality and the black square indicates the highest point along the MEP. Note that the break along the MEP is an artifact caused by the procedure employed to obtain the MEP (see Figure S7). The white circles indicate the MEP as it is obtained conventionally using a steepest descent from the TS.

whereas for energies near and below the minimum barrier QD yields a considerably lower sticking probability than QCT, which is likely to be caused by ZPE leakage in the QCT. Moreover, for the experimental sticking probability only reacted, and not trapped, molecules were taken into account. In the calculations presented in this work, trapping hardly occurs and has a negligible effect on the sticking probability. Thus, sticking and reaction probabilities (i.e., the probabilities of dissociative chemisorption) can be considered equal.

The effect of surface atom motion on the sticking probability is investigated in Figure 7. In the frozen ideal surface model,
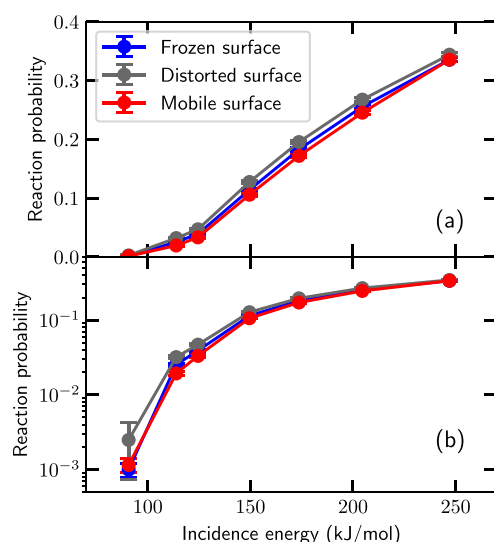

Figure 7. (a) Sticking probability of HCl on Au(111) using the MS-RPBEl functional for normal incidence and T_S = 170 K. Results employing a frozen, thermally distorted, and mobile surface are indicated by the blue, gray, and red circles, respectively. The error bars represent 68% confidence intervals. (b) Same as panel a, but using a logarithmic scale.

both the energy transfer from the molecule to the surface phonons and the thermal variation in barrier heights (due to puckering of surface atoms[79]) are excluded. The difference between the frozen and the mobile surface results is minimal, the sticking probability of the frozen surface being at most one percentage point (0.01) higher than that of the mobile surface. As previously seen for CHD$_3$ + Cu(111),[3] the effects of energy transfer and variation in barrier heights on the sticking probability are opposite and can (partially) cancel each other. This can be seen by also comparing with results obtained using a thermally distorted surface, which model takes into account the thermal variation in barrier heights, i.e., electronic and mechanical coupling, in an approximate way. The thermally distorted surface yields sticking probabilities that are at most two percentage points higher than obtained with the mobile surface. Thus, we can conclude that in the present calculation not only the total effect of surface atom motion on the sticking is small, but also its important individual components (energy transfer, and thermal barrier height and location variation), as these components taken by themselves all have a small effect on the sticking probability. We suspect that the effect of surface atom motion on the sticking of HCl on Au(111) is small because the electronic couplings between HCl and the surface atoms are smaller than for example CH$_4$ + Ni(111) by a factor 4.6[78] (see section 3.2). We also note that the electronic

coupling has a larger effect on sticking than mechanical coupling[78] and that the surface temperature is rather low (170 K).

The sticking probability of vibrationally excited ($\nu = 2, j = 1$) HCl is shown in Figure 8. The effect of vibrationally pre-
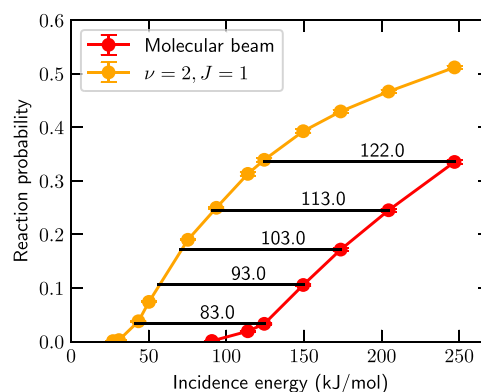

Figure 8. Sticking probability of HCl on Au(111) computed with the MS-RPBEl functional. Results for a molecular beam with the initial rovibrational population according to the nozzle temperature (see Table 2) are indicated by the red circles, and the $\nu = 2, j = 1$ initial state selected results are indicated by the orange circles. Distances between the two curves along the energy axis are indicated by the horizon black lines and numbers (kJ/mol). The error bars represent 68% confidence intervals.

exciting molecules on a reaction is typically described with the so-called vibrational efficacy $\eta(S_0)$, which is the shift in translational energy for a particular sticking probability S_0 divided by the increase in vibrational energy relative to the vibrational ground state. For $S_0 = 0.03$ the vibrational efficacy is 1.2 and for $S_0 = 0.34$ it is 1.8; i.e., vibrational energy is more efficient at promoting reaction than translational energy. This may be expected from the barrier geometry previously discussed in section 3.2 when one invokes the Polanyi rules[80] and assumes additionally that the molecule may slide off the MEP, especially for $\nu = 0$.[81−84] According to Polanyi, if the barrier is late (as is the case for HCl + Au(111)), vibrational energy may be more efficient in promoting reaction than translational energy. A similarly high value for the vibrational efficacy was previously found for $\nu_1 = 2$ CHD$_3$ + Cu(111).[3]

3.4. Dynamics during the Reaction Obtained with Theory. *3.4.1. Vibrational Excitation.* The transition probabilities for vibrationally inelastic scattering probabilities ($T_{\nu=1,j=1\rightarrow\nu=2}$ and $T_{\nu=0,j=0\rightarrow\nu=1}$) are shown in parts a and b of Figure 9, respectively. In order to directly compare the computed results with the experimental results, we define the vibrational transition probabilities as[32]

$$T_{\nu=i\rightarrow\nu=i+1} = \frac{N_{\nu=i+1}}{N_{\nu=i} + N_{\nu=i+1}} \quad (11)$$

where $N_{\nu=i}$ is the number of molecules scattered to the $\nu = i$ vibrational state. Here we discuss a few observations regarding the theoretical results.

First, the agreement between experiment and theory is improved with the MS-RPBEl functional compared with the SRP32-vdW-DF1 and RPBE functionals. Second, both modeling the effect of ehp excitation and using Gaussian binning instead of histogram binning would lower the
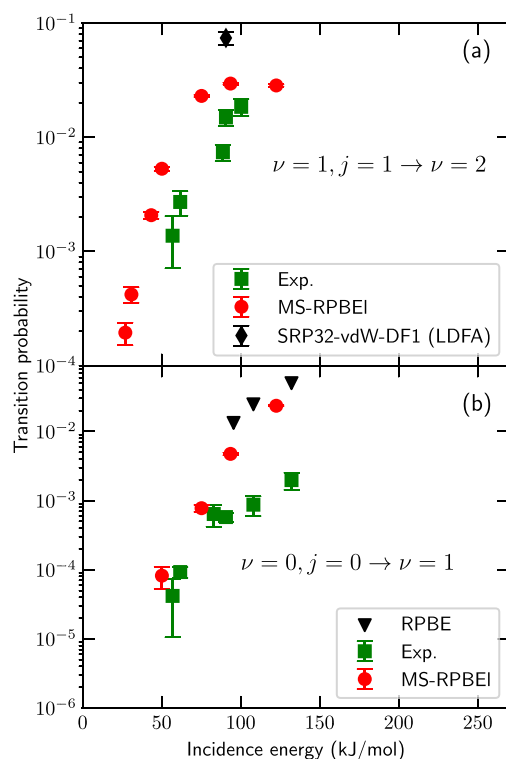
Figure 9. Vibrational transition probability computed with the MS-RPBEl functional (red circles) for $\nu = 1, j = 1 \rightarrow \nu = 2$ (a) and $\nu = 0, j = 0 \rightarrow \nu = 1$ (b) at $T_S = 170$ K for normal incidence. Experimental results[32] and their error bars were taken for the lowest T_S for which they are available; below this value of T_S the experimental transition probabilities were essentially independent of T_S. The experimental results are indicated by the green squares. Computed results using the SRP32-vdW-DF1 functional from ref 27 (black diamonds) and the RPBE functional from ref 2 (black triangles) are included as well. Note that the results obtained with the SRP32-vdW-DF1 functional employed the LDFA and assumed $T_S = 575$ K. The results using the RPBE functional employed a monoenergetic beam and assumed $T_S = 323$ K.

Figure 10. (a) Energy transfer to the surface phonons in scattering of HCl from Au(111) as a function of the incidence energy for $T_S = 170$ K. The initial rovibrational state distribution is either sampled according to the nozzle temperature (red and green) or HCl is in $\nu = 2$ and $j = 1$ state (orange and blue). Orange and blue indicate results for inelastic ($\nu = 2 \rightarrow \nu = 1$) and elastic ($\nu = 2 \rightarrow \nu = 2$) scattering, respectively. The circles and diamonds indicate results obtained with the MS-RPBEl and PBE[35] functionals, respectively. (b) Difference of the initial and final translational energy in scattering of HCl from Au(111). Experiment[29] and theory are indicated by squares and circles, respectively. Results for $\nu = 1, J = 1$ pre-excited HCl with the SRP32-vdW-DF1 functional[27] are indicated by gray triangles. The refined Baule model average (Baule limit) is indicated by the solid (dashed) black line. The experimental results are for $T_S = 300$ K, and the SRP32-vdW-DF1 results are obtained with AIMDEF calculations modeling energy transfer to the phonons as well as ehp excitations in scattering of ($\nu = 1, J = 1$) HCl for $T_S = 900$ K.

computed transition probabilities.[2] Unfortunately, it remains unclear whether ehp excitations play a major role for HCl + Au(111); to determine this, calculations modeling ehp excitation using orbital dependent friction (ODF)[22,85−88] are needed as calculations with LDFA predict only a small effect. Several binning procedures exist, and the binning procedure selected can influence the results.[42] It remains unclear what method would be best suitable, but this is not the focus of the present work. Third, the surface temperature employed in the DFMD simulations using the SRP32-vdW-DF1 functional is considerably higher ($T_S = 575$ K) than used in this work ($T_S = 170$ K), but for this temperature range experimental results suggest that the effect of T_S on the transition probability should be small.[28,32] Finally, though a difference between theory and experiment remains for absolute transition probabilities, the enhancement of the $\nu = 1, j = 1 \rightarrow \nu = 2$ channel relative to the $\nu = 0, j = 0 \rightarrow \nu = 1$ channel is approximately of the same order of magnitude.

3.4.2. Energy Transfer. The computed energy transfer from scattering HCl to the surface phonons of Au(111) is shown in Figure 10a. Results obtained by Füchsel et al. employing the PBE functional[35] are in good agreement with our results obtained with the MS-RPBEl functional. Note that the PBE results were obtained for $T_S = 298$ K, which is slightly higher
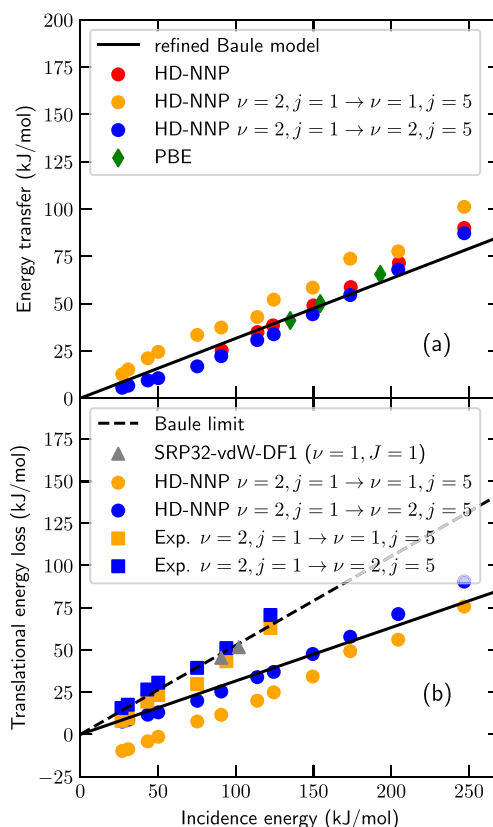
than the surface temperature in this work ($T_S = 170$ K), but also that calculations suggest that this has only a minor effect on the energy transfer.[35,36] Furthermore, simulations employing the RPBE functional resulted in about 10−15% lower energy transfer than simulations using the PBE functional.[35] Interestingly, the energy transfer predicted with the SRP32-vdW-DF1 functional[27] is about 80% higher than with the MS-RPBEl functional. Including ehp excitation hardly has any effect on the energy transfer, at least not at the LDFA level.[2,35] This suggests that van der Waals correlation increases energy transfer from the molecule to the surface phonons considerably. At present it is unknown what the underlying reason is. A possibility would be that the molecule is accelerated by the physisorption well (which effect is missing with the MS-RPBEl and (R)PBE DFs), and would thus hit the surface with a higher velocity and transfer more energy.

The energy transfer obtained from our simulations compares well with the Baule average obtained with the refined Baule model,[89,90] which is defined as

$$\langle E_T \rangle = \frac{2.4\mu}{(1+\mu)^2} \langle E_i \rangle \tag{12}$$

where $\mu = m/M$ (m is the mass of the projectile and M is the mass of a surface atom) and $\langle E_i \rangle$ is the average incidence energy. Good agreement between the refined Baule model and computed energy transfer has also been observed for several other systems such as CHD_3 and methanol scattering from Cu(111), Pd(111), and Pt(111).[64,90,91] Füchsel et al. reported that the Baule model severely overestimated the energy transfer for HCl scattering from Au(111)[35] while employing GGA functionals without van der Waals correlation. However, the comparison was made with the more approximate Baule limit, where every collision is treated as a head-on collision, which could overestimate the energy transfer as this is a rather severe approximation. As we have shown in Figure 10a the PBE results obtained in ref.[35] are instead in good agreement with the refined Baule model average, which is lower than the Baule limit. However, the energy transfer predicted with the SRP32-vdW-DF1 functional compares well with that obtained in the Baule limit.

A comparison between theory (with the MS-RPBEl functional)[29] and experiment[29] is made in Figure 10b for the change in translational energy (i.e., the loss of translational energy). Note that the ordering of vibrationally elastic and inelastic scattering has switched here compared to Figure 10a due to the fact that in Figure 10b we look at translational energy loss, which also arises from energy transfer involving molecular rotation and vibration, and not at the energy transfer to the phonons only. A qualitative agreement is obtained for the translational energy loss, but not a quantitative one. As expected vibrational de-excitation is accompanied by a smaller loss in translational energy than vibrationally elastic scattering as some of the vibrational energy loss will be transferred to translational energy (V-T, Figure 10b). Likewise, for vibrational de-excitation a larger energy transfer from the molecule to the surface is observed than for vibrationally elastic scattering since part of the vibrational energy loss will be transferred to the phonons (V-P, Figure 10a). Interestingly, the experimental results suggest that the Baule limit, and not the Baule average, is an accurate prediction for the energy transfer, if one compares the elastic scattering results to the Baule limit (i.e., no vibrational energy transfer and little effect from rotational energy transfer). Since the SRP32-vdW-DF1 AIMDEF results also compare well to the Baule limit, van der Waals correlation and modeling energy transfer to ehps might both be necessary to accurately model energy transfer between HCl and Au(111).

Figure 11 shows the average translational energy of vibrationally (in)elastically scattered HCl from Au(111) as a function of the final rotational quantum number. Again, only a qualitative agreement is obtained between experiment and theory in the sense that the trends are recovered that vibrationally de-excited HCl retains more translational energy and that the final translational energy of vibrationally de-excited HCl shows a weaker dependence on its final rotational state. It is likely that the aforementioned lack of van der Waals correlation in this work causes at least part of the quantitative difference between experiment and theory. The decrease in translational energy with increasing rotational quantum
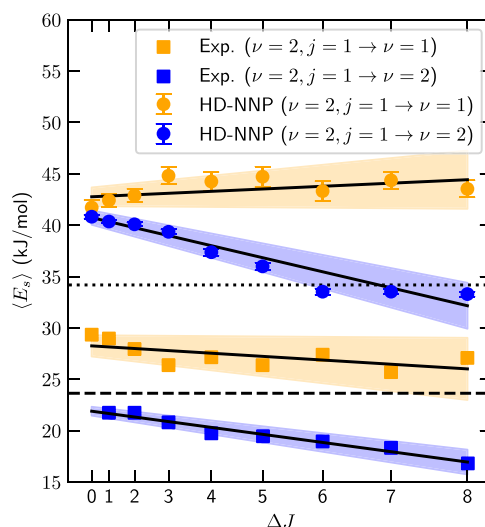

Figure 11. Average translational energy of HCl scattered from Au(111) as a function of change in rotational state for $\langle E_i \rangle = 50$ kJ/mol. The initial rovibrational state is $\nu = 2$ and $j = 1$ and the final vibrational state is $\nu = 1$ or $\nu = 2$ (orange and blue, respectively). Experimental[29] and theoretical results are indicated by squares and circles, respectively. The solid black lines are linear regression lines fitted to the results and the blue and orange shaded areas are the 2σ (95%) confidence intervals of those fits. The dotted (dashed) black line is the refined Baule model average (Baule limit). The error bars represent 68% confidence intervals.

number is due to translational energy being transferred to rotational energy. Although it seems as if an increase in translational energy with increasing final rotational energy is predicted by theory for vibrationally inelastic scattering ($\nu = 2 \rightarrow \nu = 1$), it is possible that this is a statistical anomaly due to limited statistics (see Figure 11 and the 2σ confidence intervals therein). After making comparisons to the Baule model, coupling of the projectile's translation to the ehps of the solid was previously suggested.[29] This is the first time a high quality first-principles adiabatic theory has been compared to these experiments. The fact that the difference between the computed translational energy of elastic and inelastic scattered HCl is smaller than that obtained by experiment tends to confirm the suggestions of ref 29.

The effect of the impact site on the energy transfer is visualized in Figure 12. Two observations stand out: More energy is transferred to the surface atoms in collisions with the hollow and bridge sites, and, when considering only collisions with the area assigned to the top site, more energy is transferred in (head-on) collisions with the actual top site than in collisions that have a larger impact parameter with respect to the top site. The latter observation is in agreement with the Baule model, but the former observation is not. It is possible that while the energy transfer near a hollow or bridge site with a single surface atom is comparable to that of the top site (i.e., is in agreement with the Baule model), the molecule interacts with multiple surface atoms in a single collision and therefore the total energy transfer is larger near the hollow and bridge sites than near the top site. These multiple molecule–surface interactions cannot be evaluated within a single collision in the Baule model, as one might do by artificially increasing the surface atom mass in eq 12 since this would actually lower the energy transfer. Thus, we conclude that the Baule model is too simplistic for a good qualitative description of the energy
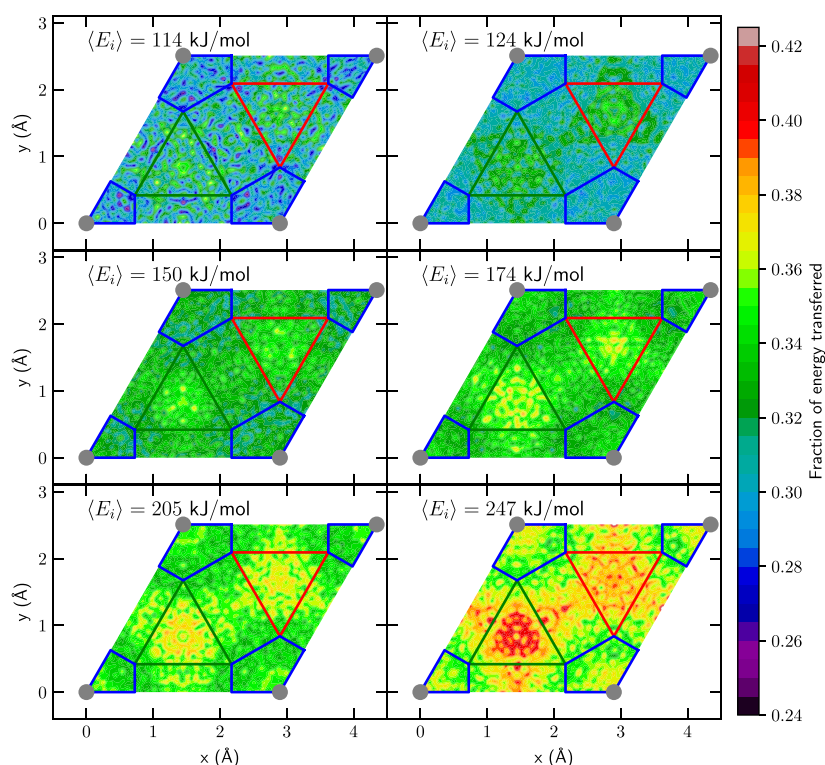
Figure 12. Fraction of the translational energy of scattered HCl transferred to the surface phonons of Au(111) as a function of the initial impact site ($t = 0$) on the surface unit cell and incidence energy. The areas enclosed by the blue, green, and red lines are the areas closest to the top, fcc, and hcp sites, while the rest is closest to the bridge site.

transfer. Also, a model where the energy transfer is modeled within a simplistic single oscillator model, such as the generalized Langevin oscillator (GLO) model,[92] would probably also incorrectly describe the energy transfer of HCl to Au(111) since such a model would also rely on energy transfer to a single surface oscillator at a given specific time, and not to more than one surface atom simultaneously. Furthermore, in the introduction of the modified GLO model it was suggested that its accuracy can be improved by including not only the Z location in the coupling potential, but also the X and Y coordinates.[93] However, for HCl + Au(111) the mechanical and electronic coupling is not only dependent on the position of the COM (i.e., X, Y and Z) but also on the orientation (i.e., θ and ϕ). Therefore, it is likely that an accurate description of HCl + Au(111) using the MGLO model would require a coupling potential depending on all HCl's six degrees of freedom.

3.4.3. Site Specific Reaction. The dynamical steering of reacting and scattering HCl on Au(111) (i.e., change in the projection of the COM of HCl on the surface during trajectories) in the XY direction is shown in Figure 13. For reacting HCl, the distance is shown between the initial XY position and the XY position at the moment of reaction ($r = r^{\ddagger}$) of the COM of HCl. For scattering HCl, instead of the XY position at the moment of reaction ($r = r^{\ddagger}$), the XY position is taken at the first classical turning point in the Z direction. For reacting HCl slightly more steering is observed than for scattering HCl, but in any case for both processes the amount of steering is fairly small. Therefore, a sudden impact model[94] regarding the X and Y positions should be sufficient for modeling the reaction. This was also observed by Liu et al.,[30] who showed that a model in which 4D sticking results are averaged over several fixed locations of X and Y, i.e., the COM
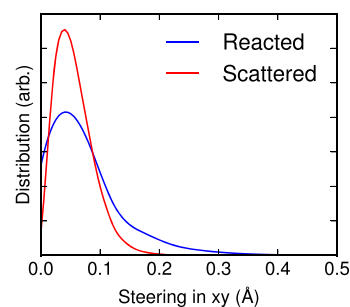

Figure 13. Steering of HCl in the XY plane when reacting on or scattering from Au(111) (blue and red line, respectively). For scattering HCl, the steering is defined as the distance between the location of the COM in the XY plane at the first classical turning point in the Z direction and its location at $t = 0$. For reacting HCl, the locations in the XY plane are taken at the moment of reaction ($r = r^{\ddagger}$) and at $t = 0$.

of the molecule cannot move in the X and Y directions, can accurately reproduce 6D sticking probabilities, as long as enough sites are included.

The importance of the impact site for the sticking can also be seen in Figure 14, where the sticking probability is shown as a function of impact site. At low incidence energy reaction occurs mostly near the bridge site, followed by the hollow and top site. At high incidence energy the hollow site becomes relatively more reactive and reaction occurs equally near the bridge and hollow sites, while the top site is still considerably less reactive. Interestingly, from the barrier heights in Table 5 it is expected that the hollow site should be the least reactive site, while the top site should be considerably more reactive. Additionally, a site with a barrier that is earlier (i.e., has a lower
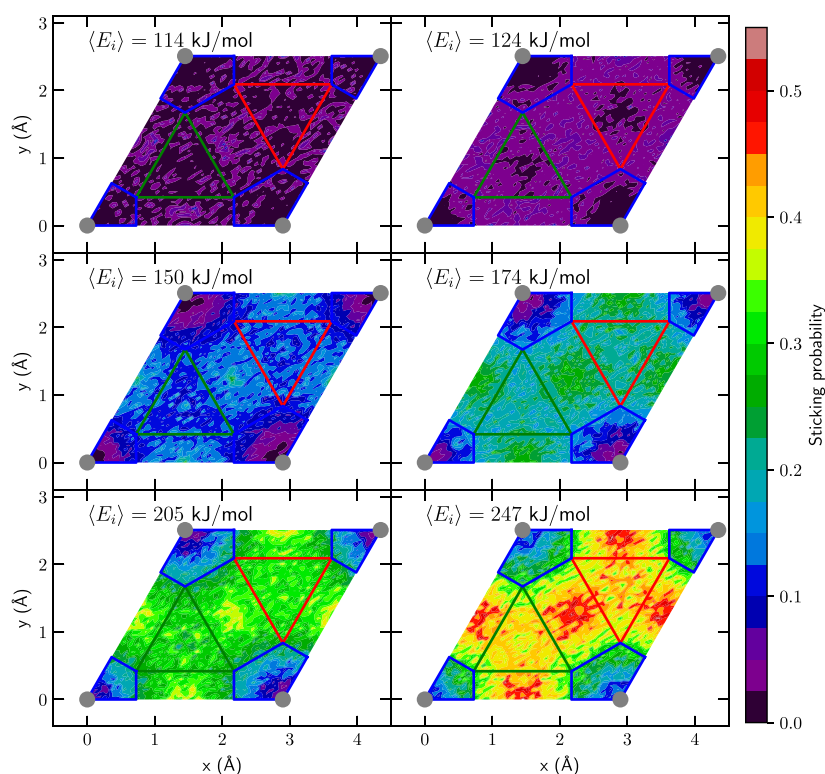
Figure 14. Sticking probability of HCl on Au(111) as a function of the initial impact site ($t = 0$) of the COM on the surface unit cell and incidence energy. The areas enclosed by the blue, green, and red lines are the areas closest to the top, fcc, and hcp sites, while the rest is closest to the bridge site.

r value, like the top site) is often more reactive. Our results suggest that these particular static aspects of the PES (barrier height and geometry) do not play a very large role, as the hollow site is clearly more reactive than the top site.

Since the impact sites considered in Figure 14 differ in the shape of the MEP (see Figure 4), one might expect that the bobsled effect plays a role. In the bobsled effect, the molecule slides off the MEP up the repulsive wall, if the MEP has a too sharp turn compared to the translational energy of the molecule, so that the molecule encounters a higher barrier than the minimum barrier.[81,82] Although Figure 15 strongly suggests that the bobsled effect does play a role overall (as the molecules appear to react much closer to the surface than suggested by the location of the minimum barrier), if anything the observations suggest that the negative impact on the reactivity should be largest in collisions with the bridge and hollow sites. Thus, the bobsled effect cannot explain the variation of reactivity with impact site.

It is known that the molecule might not be able to react over the minimum barrier if it is dynamically inaccessible, e.g., as observed for the dissociation of HOD on Ni(111).[95] We hypothesized in section 3.2 (see also Figures 4 and 5) that the top site barrier might be dynamically less accessible due to the shape of the MEP. Furthermore, it is possible that due to the different site specific dependence of the potential on θ and ϕ (the polar and azimuthal angles, respectively), the site specific reactivity might be affected differently depending on the anisotropy in the θ and ϕ angles (see Figure S8). These observations are also supported by the site specific reaction probabilities obtained by Liu et al. employing the PW91 functional and QD:[30] Top site reaction favors a cartwheel orientation (steering in θ), bridge site reaction favors a
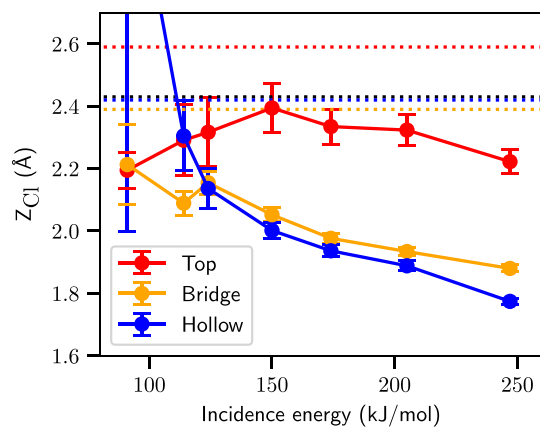

Figure 15. Distance between Cl and the surface (Z_{Cl}) for HCl reacting on Au(111) near the top, bridge and hollow sites (red, orange, and blue, respectively) at the moment of reaction ($r = r^{\ddagger}$, see Table 5) using the MS-RPBEl functional. The sites are determined as the nearest high symmetry site for a reacted trajectory at $t = 0$. The dashed lines indicate the values associated with the minimum barriers at these sites, while the global TS is indicated by the black line.

helicopter orientation (steering in ϕ), and hollow site reaction shows no clear preference. A large amount of steering in the θ angle is seen in Figure 16, where the orientation distributions of scattering and reacting HCl are shown. Moreover, the initial angular distributions are statistical. Thus, we conclude that the observed site specific reactivity is probably due to the dynamical accessibility of the barriers. Furthermore, if the initial angular distribution that leads to reaction is statistical and concomitant steering is observed, typically a rotationally adiabatic approximation should be adequate.[94]
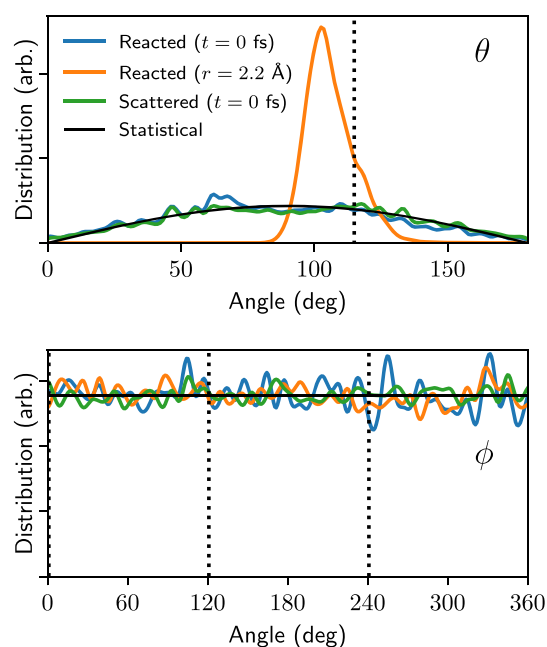
Figure 16. Distribution of θ and ϕ angles for HCl on Au(111). The distributions at the initial time step ($t = 0$) for reacted and scattered HCl are indicated in blue and green, respectively, whereas the distribution for reacted HCl at the moment of reaction ($r = 2.2$ Å) is indicated in orange. The statistical distribution is indicated by the solid black line, and the values from the global TS are indicated by the dotted black line.

Figure 17 again shows the site specificity of the reaction. The upper panel shows clearly that more molecules react at the
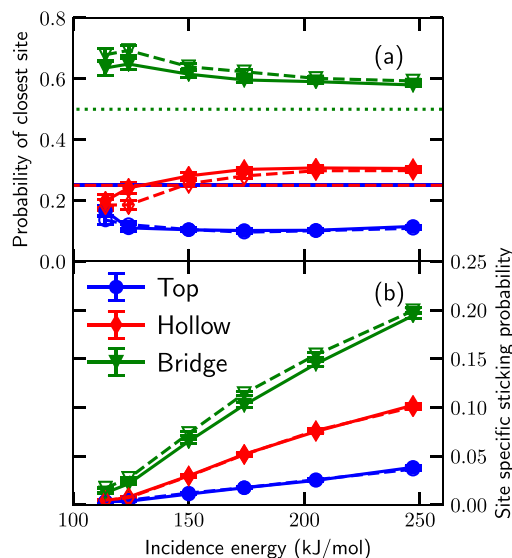

Figure 17. (a) Fractions of the closest high symmetry sites encountered by HCl, i.e., the top, hollow, and bridge (blue, red, and green, respectively) sites, as a function of the incidence energy at the time of dissociation, that is, when $r = r^{\ddagger}$. The dashed and dotted lines indicate the statistical average for the high symmetry sites. The open and solid symbols indicate the use of a frozen and mobile surface, respectively. (b) Sticking probability of HCl on the high symmetry sites as a function of the incidence energy. Note that the site specific sticking probabilities add up to the total sticking probability. The error bars represent 68% confidence intervals.

bridge site than expected on the basis of the area associated with this site (see Figure 14 for how the surface unit cell is partitioned), while fewer molecules react at the top site than expected on this basis. The lower panel shows that overall most molecules react at the bridge site, followed by the hollow and top sites. We also observe that if a frozen surface is employed instead of a mobile surface, i.e., if energy transfer and the thermal variation of barrier heights are not taken into account, only the bridge site becomes more reactive.

Additionally, for $\nu = 2$ vibrationally excited HCl a statistical site specific reactivity is obtained for $S_0 > 0.2$ (see Figure S4). In contrast, for $S_0 < 0.2$, the site specific reactivity is nonstatistical, but it does not follow the trend of the barrier heights in Table 5 either, nor is the state specificity similar to that found under molecular beam conditions. Rather, the order of the sites in terms of reactivity is now top > bridge > hollow. This observation implies that adding vibrational energy increases the dynamical accessibility of specific barriers, especially that of the top site.

4. ADDITIONAL DISCUSSION

A considerable disagreement between theory and experiment remains, even though the difference between the two is diminishing. Here we will discuss a few remaining issues that could potentially explain the difference between theory and experiment for sticking and vibrationally inelastic scattering.

First, experience suggests that including ehp excitations with the LDFA will not yield a substantially improved description of the sticking probability. Description of ehp excitation with a higher level of theory such as independent electron surface hopping[96,97] or ODF[22,85−88] might improve the results. Since dynamical steering is important for the reaction of HCl on Au(111) and ODF has been observed to alter the dynamics,[87] modeling ehp excitation with ODF might have a larger effect on the sticking probability than modeling ehp excitation at the LDFA level of theory. Indeed, there is some evidence now that the translational motion of the HCl molecule may be able to excite ehps of Au. This could reduce the reactivity since translational energy is necessary to surmount the barrier.

Second, experimentally not an ideal (111) surface is employed, but a reconstructed herringbone patterned surface. Such a surface reconstruction is well-known to occur for gold, and might alter the reactivity of the surface.[98] Unfortunately, the surface unit cell associated with such a reconstruction is quite large, making tractable MD simulations difficult. An embedded atom model might make such MD simulations tractable,[99] but this might lead to loss of accuracy of the molecule-metal surface interaction.

Furthermore, the presence or absence of a physisorption well can influence the dynamics[100] and therefore the reactivity as well, even when the barrier height is similar (e.g., CHD_3 + Pt(111) using the PBE and SRP32-vdW-DF1 DFs[101]). Therefore, it is possible that adding van der Waals correlation to the MS-RPBEl functional might lower the sticking probability even further. Also, it is likely that the discrepancy between the measured and computed energy transfer will be diminished by using van der Waals correlation (see section 3.4.2). Moreover, the use of the nonlocal vdW-DF2 correlation[102] instead of the vdW-DF1 correlation typically increases the barrier height,[8,103] and might therefore improve the description of HCl + Au(111) compared to that previously obtained with vdW-DF1.[27]

Fourth, and probably most importantly, Füchsel et al. have shown that a considerable amount of charge transfer occurs when HCl is near the surface with the use of the (R)PBE DFs.[35] Since GGA functionals suffer from delocalization errors (due to SIE), the barrier height might be artificially lowered when employing DFs that suffer from SIE. For example, compared to standard GGA DFs, the embedded correlation wave function method and (range-separated) hybrid DFs yield considerably better sticking probabilities and/or barriers for O_2 + Al(111),[7,15,16,24,104,105] a system known for a large charge transfer. In this framework it is highly significant that the DF used here to describe the interaction between HCl and Au(111), which was explicitly designed to correct for SIE at the meta-GGA level of theory, yields significantly improved results for this system compared to results obtained earlier using GGA exchange functionals. Future work involving advanced methods that would remedy the SIE at a higher level of theory could perhaps further increase the barrier height of HCl dissociating on Au(111) and lead to further improved computed sticking probabilities.

As has been briefly mentioned in section 3.4.1, the binning method can influence the rovibrational state populations obtained. Thus, a combined QCT and QD study that would investigate the binning method is necessary. We do note that a change in sticking probability due to the use of a different binning method, as has recently been observed by Rodríguez et al.[42] for H_2 + Pd(111), is not expected here. For H_2 + Pd(111) only the vibrational ground state and a few rotational states are available, and analyzing the QCT sticking probabilities in a quantum spirit is necessary. In contrast, for HCl + Au(111) many rovibrational states are available, making the use of quasi-classical theory with histogram binning in the analysis of the QCT calculations justified.[43] Moreover, QD and AIMD calculations performed with the RPBE DF lead to similar sticking probabilities.[37]

Turning to scattering, the (in)elastic scattering experiments were performed only for a final scattering angle of 15°,[32] whereas in our simulations all scattering angles are taken into account. However, the experimental results are corrected in such a way that they should yield the average over the entire angular distribution, where this correction is valid when no significant difference in angular distribution between different rotational states exist.[32] Also, the experimental incidence angle is between 0° and 5°, while the simulations are performed for normal incidence, i.e., the incidence angle is 0°. However, results by Füchsel et al.[35] suggest that this has only a minor effect on the energy transfer of HCl scattering from Au(111). In this work, for the vibrational transition probabilities a larger effect of the scattering angle is observed (see Figure S5): The vibrational transition probabilities ($T_{\nu=1,j=1\rightarrow\nu=2}$) are increased by a factor of 1.2 for low incidence energy up to a factor of 2.3 for high incidence energy, resulting in a larger discrepancy between experiment and theory. Qualitatively similar results are expected when employing other DFs and thus we expect that the MS-RPBEl would also yield the best agreement between experiment and theory for the excitation probabilities if the theoretical results for the other DFs would also be obtained for a restricted range of scattering angles, as done by us.

Finally, as we have shown in this work, a large uncertainty regarding the experimental sticking probabilities remains. Future experiments reducing the uncertainty would help with testing theory, but first theory should be brought into better

agreement with experiment. Furthermore, molecular beam studies where HCl is state-selectively prepared with laser excitation could serve as an improved benchmark for theory. Not only might such studies provide potentially more accurate sticking probabilities since they might be easier to measure but also vibrational efficacies could be compared. Experiments like this are in an early preparation stage.

5. CONCLUSIONS

To summarize, in this work, the dissociative chemisorption of HCl on Au(111) is reinvestigated with molecular dynamics and a high-dimensional neural network potential and previous experiments are re-examined to better characterize their error margins. By employing a recently developed MGGA DF (MS-RPBEl) and reanalyzing the experimental data, the agreement between computed and measured sticking probabilities is improved considerably. The computed minimum barrier height is high (100.6 kJ/mol) and the barrier geometry is late (i.e., the HCl bond is extended from 1.28 Å in the gas phase to 2.18 Å at the transition state), which results in a decrease of the sticking probability relative to dynamics calculations based on the other DFs tested so far. Furthermore, surface atom motion is found to be of minor influence on the sticking probability. Moreover, computed and measured vibrational transition probabilities are also in improved agreement, although the employed binning method warrants additional research. Dynamical effects, like rotational steering, play an important role in the overall reactivity, leading to a dependence of the reactivity on impact sites that cannot be explained on the basis of site-specific barrier heights and locations. A qualitative, but not quantitative agreement between experiment and theory is obtained for the energy transfer of the HCl molecule to the surface. Finally, we discussed a number of possibilities that might account for the remaining deviation between experiment and theory.

■ ASSOCIATED CONTENT

ⓈI Supporting Information

The Supporting Information is available free of charge at https://pubs.acs.org/doi/10.1021/acs.jpcc.0c03756.

> Convergence tests of computational setup and neural network, description of the symmetry functions, site specific reactivity of $\nu = 2$, $J = 1$ rovibrationally excited HCl, scattering angle and beam parameter dependence of vibrational transition probabilities, θ and ϕ dependence of site specific barrier heights, and description of the construction of the MEP (PDF)

■ AUTHOR INFORMATION

Corresponding Authors

Nick Gerrits − *Gorlaeus Laboratories, Leiden Institute of Chemistry, Leiden University, 2300 RA Leiden, The Netherlands;* ⓞ orcid.org/0000-0001-5405-7860; Email: n.gerrits@lic.leidenuniv.nl

Geert-Jan Kroes − *Gorlaeus Laboratories, Leiden Institute of Chemistry, Leiden University, 2300 RA Leiden, The Netherlands;* ⓞ orcid.org/0000-0002-4913-4689; Email: g.j.kroes@chem.leidenuniv.nl

Authors

Jan Geweke − *Max Planck Institute for Biophysical Chemistry, Göttingen, 37077 Göttingen, Germany; Institute for Physical Chemistry, University of Göttingen, 37077 Göttingen, Germany*

Egidius W. F. Smeets − *Gorlaeus Laboratories, Leiden Institute of Chemistry, Leiden University, 2300 RA Leiden, The Netherlands;* orcid.org/0000-0003-0111-087X

Johannes Voss − *SLAC National Accelerator Laboratory, SUNCAT Center for Interface Science & Catalysis, Menlo Park, California 94025, United States;* orcid.org/0000-0001-7740-8811

Alec M. Wodtke − *Max Planck Institute for Biophysical Chemistry, Göttingen, 37077 Göttingen, Germany; Institute for Physical Chemistry and International Center for Advanced Studies of Energy Conversion, University of Göttingen, 37077 Göttingen, Germany;* orcid.org/0000-0002-6509-2183

Complete contact information is available at:
https://pubs.acs.org/10.1021/acs.jpcc.0c03756

Notes

The authors declare no competing financial interest.

■ REFERENCES

(1) Shakouri, K.; Behler, J.; Meyer, J.; Kroes, G.-J. Accurate Neural Network Description of Surface Phonons in Reactive Gas−Surface Dynamics: N_2 + Ru(0001). *J. Phys. Chem. Lett.* 2017, 8, 2131−2136.

(2) Liu, Q.; Zhou, X.; Zhou, L.; Zhang, Y.; Luo, X.; Guo, H.; Jiang, B. Constructing High-Dimensional Neural Network Potential Energy Surfaces for Gas−Surface Scattering and Reactions. *J. Phys. Chem. C* 2018, 122, 1761−1769.

(3) Gerrits, N.; Shakouri, K.; Behler, J.; Kroes, G.-J. Accurate Probabilities for Highly Activated Reaction of Polyatomic Molecules on Surfaces Using a High-Dimensional Neural Network Potential: CHD_3 + Cu(111). *J. Phys. Chem. Lett.* 2019, 10, 1763−1768.

(4) Zhang, Y.; Zhou, X.; Jiang, B. Bridging the Gap between Direct Dynamics and Globally Accurate Reactive Potential Energy Surfaces Using Neural Networks. *J. Phys. Chem. Lett.* 2019, 10, 1185−1191.

(5) Yin, R.; Zhang, Y.; Jiang, B. Strong Vibrational Relaxation of NO Scattered from Au(111): Importance of the Adiabatic Potential Energy Surface. *J. Phys. Chem. Lett.* 2019, 10, 5969−5974.

(6) Díaz, C.; Pijper, E.; Olsen, R. A.; Busnengo, H. F.; Auerbach, D. J.; Kroes, G. J. Chemically Accurate Simulation of a Prototypical Surface Reaction: H_2 Dissociation on Cu(111). *Science* 2009, 326, 832−834.

(7) Liu, H.-R.; Xiang, H.; Gong, X. G. First Principles Study of Adsorption of O_2 on Al Surface with Hybrid Functionals. *J. Chem. Phys.* 2011, 135, 214702.

(8) Wijzenbroek, M.; Kroes, G. J. The Effect of the Exchange-Correlation Functional on H_2 Dissociation on Ru(0001). *J. Chem. Phys.* 2014, 140, 084702.

(9) Nattino, F.; Migliorini, D.; Kroes, G.-J.; Dombrowski, E.; High, E. A.; Killelea, D. R.; Utz, A. L. Chemically Accurate Simulation of a Polyatomic Molecule-Metal Surface Reaction. *J. Phys. Chem. Lett.* 2016, 7, 2402−2406.

(10) Migliorini, D.; Chadwick, H.; Nattino, F.; Gutiérrez-González, A.; Dombrowski, E.; High, E. A.; Guo, H.; Utz, A. L.; Jackson, B.; Beck, R. D.; et al. Surface Reaction Barriometry: Methane Dissociation on Flat and Stepped Transition-Metal Surfaces. *J. Phys. Chem. Lett.* 2017, 8, 4177−4182.

(11) Zhou, X.; Jiang, B.; Guo, H. Dissociative Chemisorption of Methane on Stepped Ir(332) Surface: Density Functional Theory and Ab Initio Molecular Dynamics Studies. *J. Phys. Chem. C* 2019, 123, 20893−20902.

(12) Ghassemi, E. N.; Smeets, E. W. F.; Somers, M. F.; Kroes, G.-J.; Groot, I. M. N.; Juurlink, L. B. F.; Füchsel, G. Transferability of the Specific Reaction Parameter Density Functional for H_2 + Pt(111) to H_2 + Pt(211). *J. Phys. Chem. C* 2019, 123, 2973−2986.

(13) Lončarić, I.; Alducin, M.; Juaristi, J. I.; Novko, D. CO Stretch Vibration Lives Long on Au(111). *J. Phys. Chem. Lett.* 2019, 10, 1043−1047.

(14) Smeets, E. W. F.; Voss, J.; Kroes, G.-J. Specific Reaction Parameter Density Functional Based on the Meta-Generalized Gradient Approximation: Application to H_2 + Cu(111) and H_2 + Ag(111). *J. Phys. Chem. A* 2019, 123, 5395−5406.

(15) Libisch, F.; Huang, C.; Liao, P.; Pavone, M.; Carter, E. A. Origin of the Energy Barrier to Chemical Reactions of O_2 on Al(111): Evidence for Charge Transfer, Not Spin Selection. *Phys. Rev. Lett.* 2012, 109, 198303.

(16) Yin, R.; Zhang, Y.; Libisch, F.; Carter, E. A.; Guo, H.; Jiang, B. Dissociative Chemisorption of O_2 on Al(111): Dynamics on a Correlated Wave-Function-Based Potential Energy Surface. *J. Phys. Chem. Lett.* 2018, 9, 3271−3277.

(17) Blanco-Rey, M.; Juaristi, J. I.; Díez Muiño, R.; Busnengo, H. F.; Kroes, G. J.; Alducin, M. Electronic Friction Dominates Hydrogen Hot-Atom Relaxation on Pd(100). *Phys. Rev. Lett.* 2014, 112, 103203.

(18) Janke, S. M.; Auerbach, D. J.; Wodtke, A. M.; Kandratsenka, A. An Accurate Full-Dimensional Potential Energy Surface for H−Au(111): Importance of Nonadiabatic Electronic Excitation in Energy Transfer and Adsorption. *J. Chem. Phys.* 2015, 143, 124708.

(19) Rittmeyer, S. P.; Meyer, J.; Juaristi, J. I.; Reuter, K. Electronic Friction-Based Vibrational Lifetimes of Molecular Adsorbates: Beyond the Independent-Atom Approximation. *Phys. Rev. Lett.* 2015, 115, 046102.

(20) Bünermann, O.; Jiang, H.; Dorenkamp, Y.; Kandratsenka, A.; Janke, S.; Auerbach, D. J.; Wodtke, A. M. Electron-Hole Pair Excitation Determines the Mechanism of Hydrogen Atom Adsorption. *Science* 2015, 350, 1346−1349.

(21) Kandratsenka, A.; Jiang, H.; Dorenkamp, Y.; Janke, S. M.; Kammler, M.; Wodtke, A. M.; Bünermann, O. Unified Description of H-Atom− Induced Chemicurrents and Inelastic Scattering. *Proc. Natl. Acad. Sci. U. S. A.* 2018, 115, 680−684.

(22) Spiering, P.; Shakouri, K.; Behler, J.; Kroes, G.-J.; Meyer, J. Orbital-Dependent Electronic Friction Significantly Affects the Description of Reactive Scattering of N_2 from Ru(0001). *J. Phys. Chem. Lett.* 2019, 10, 2957−2962.

(23) Zhou, X.; Kolb, B.; Luo, X.; Guo, H.; Jiang, B. Ab Initio Molecular Dynamics Study of Dissociative Chemisorption and Scattering of CO_2 on Ni(100): Reactivity, Energy Transfer, Steering Dynamics, and Lattice Effects. *J. Phys. Chem. C* 2017, 121, 5594−5602.

(24) Sun, S.; Xu, P.; Ren, Y.; Tan, X.; Li, G. First-Principles Study of Dissociation Processes of O_2 Molecular on the Al (111) Surface. *Curr. Appl. Phys.* 2018, 18, 1528−1533.

(25) Gerrits, N.; Kroes, G.-J. Curious Mechanism of the Dissociative Chemisorption of Ammonia on Ru(0001). *J. Phys. Chem. C* 2019, 123, 28291−28300.

(26) Chadwick, H.; Gutiérrez-González, A.; Beck, R. D.; Kroes, G.-J. CHD_3 Dissociation on the Kinked Pt(210) Surface: A Comparison of Experiment and Theory. *J. Phys. Chem. C* 2019, 123, 14530−14539.

(27) Füchsel, G.; Zhou, X.; Jiang, B.; Juaristi, J. I.; Alducin, M.; Guo, H.; Kroes, G.-J. Reactive and Nonreactive Scattering of HCl from Au(111): An Ab Initio Molecular Dynamics Study. *J. Phys. Chem. C* **2019**, *123*, 2287−2299.

(28) Ran, Q.; Matsiev, D.; Auerbach, D. J.; Wodtke, A. M. Observation of a Change of Vibrational Excitation Mechanism with Surface Temperature: HCl Collisions with Au(111). *Phys. Rev. Lett.* **2007**, *98*, 237601.

(29) Rahinov, I.; Cooper, R.; Yuan, C.; Yang, X.; Auerbach, D. J.; Wodtke, A. M. Efficient Vibrational and Translational Excitations of a Solid Metal Surface: State-to-State Time-of-Flight Measurements of HCl(ν = 2,J = 1) Scattering from Au(111). *J. Chem. Phys.* **2008**, *129*, 214708.

(30) Liu, T.; Fu, B.; Zhang, D. H. Six-Dimensional Quantum Dynamics Study for the Dissociative Adsorption of HCl on Au(111) Surface. *J. Chem. Phys.* **2013**, *139*, 184705.

(31) Liu, T.; Fu, B.; Zhang, D. H. Six-Dimensional Quantum Dynamics Study for the Dissociative Adsorption of DCl on Au(111) Surface. *J. Chem. Phys.* **2014**, *140*, 144701.

(32) Geweke, J.; Shirhatti, P. R.; Rahinov, I.; Bartels, C.; Wodtke, A. M. Vibrational Energy Transfer near a Dissociative Adsorption Transition State: State-to-State Study of HCl Collisions at Au(111). *J. Chem. Phys.* **2016**, *145*, 054709.

(33) Kolb, B.; Guo, H. Communication: Energy Transfer and Reaction Dynamics for DCl Scattering on Au(111): An Ab Initio Molecular Dynamics Study. *J. Chem. Phys.* **2016**, *145*, 011102.

(34) Shirhatti, P. R.; Geweke, J.; Steinsiek, C.; Bartels, C.; Rahinov, I.; Auerbach, D. J.; Wodtke, A. M. Activated Dissociation of HCl on Au(111). *J. Phys. Chem. Lett.* **2016**, *7*, 1346−1350.

(35) Füchsel, G.; del Cueto, M.; Díaz, C.; Kroes, G.-J. Enigmatic HCl + Au(111) Reaction: A Puzzle for Theory and Experiment. *J. Phys. Chem. C* **2016**, *120*, 25760−25779.

(36) Kolb, B.; Luo, X.; Zhou, X.; Jiang, B.; Guo, H. High-Dimensional Atomistic Neural Network Potentials for Molecule−Surface Interactions: HCl Scattering from Au(111). *J. Phys. Chem. Lett.* **2017**, *8*, 666−672.

(37) Liu, T.; Fu, B.; Zhang, D. H. HCl Dissociating on a Rigid Au(111) Surface: A Six-Dimensional Quantum Mechanical Study on a New Potential Energy Surface Based on the RPBE Functional. *J. Chem. Phys.* **2017**, *146*, 164706.

(38) Perdew, J. P.; Burke, K.; Ernzerhof, M. Generalized Gradient Approximation Made Simple. *Phys. Rev. Lett.* **1996**, *77*, 3865.

(39) Perdew, J. P.; Chevary, J. A.; Vosko, S. H.; Jackson, K. A.; Pederson, M. R.; Singh, D. J.; Fiolhais, C. Atoms, Molecules, Solids, and Surfaces: Applications of the Generalized Gradient Approximation for Exchange and Correlation. *Phys. Rev. B: Condens. Matter Mater. Phys.* **1992**, *46*, 6671−6687.

(40) Hammer, B.; Hansen, L. B.; Nørskov, J. K. Improved Adsorption Energetics within Density-Functional Theory Using Revised Perdew-Burke-Ernzerhof Functionals. *Phys. Rev. B: Condens. Matter Mater. Phys.* **1999**, *59*, 7413−7421.

(41) Juaristi, J. I.; Alducin, M.; Muíño, R. D.; Busnengo, H. F.; Salin, A. Role of Electron-Hole Pair Excitations in the Dissociative Adsorption of Diatomic Molecules on Metal Surfaces. *Phys. Rev. Lett.* **2008**, *100*, 116102.

(42) Rodríguez-Fernández, A.; Bonnet, L.; Crespos, C.; Larrégaray, P.; Díez Muiño, R. When Classical Trajectories Get to Quantum Accuracy: The Scattering of H₂ on Pd(111). *J. Phys. Chem. Lett.* **2019**, *10*, 7629−7635.

(43) Bonnet, L. Classical Dynamics of Chemical Reactions in a Quantum Spirit. *Int. Rev. Phys. Chem.* **2013**, *32*, 171−228.

(44) Crespos, C.; Decock, J.; Larrégaray, P.; Bonnet, L. Classical Molecule−Surface Scattering in a Quantum Spirit: Application to H₂/Pd(111) Nonactivated Sticking. *J. Phys. Chem. C* **2017**, *121*, 16854−16863.

(45) Ran, Q.; Matsiev, D.; Wodtke, A. M.; Auerbach, D. J. An Advanced Molecule-Surface Scattering Instrument for Study of Vibrational Energy Transfer in Gas-Solid Collisions. *Rev. Sci. Instrum.* **2007**, *78*, 104104.

(46) Perdew, J. P.; Ruzsinszky, A.; Csonka, G. I.; Constantin, L. A.; Sun, J. Workhorse Semilocal Density Functional for Condensed Matter Physics and Quantum Chemistry. *Phys. Rev. Lett.* **2009**, *103*, 026403.

(47) Perdew, J. P.; Ruzsinszky, A.; Constantin, L. A.; Sun, J.; Csonka, G. I. Some Fundamental Issues in Ground-State Density Functional Theory: A Guide for the Perplexed. *J. Chem. Theory Comput.* **2009**, *5*, 902−908.

(48) Mallikarjun Sharada, S.; Karlsson, R. K. B.; Maimaiti, Y.; Voss, J.; Bligaard, T. Adsorption on Transition Metal Surfaces: Transferability and Accuracy of DFT Using the ADS41 Dataset. *Phys. Rev. B: Condens. Matter Mater. Phys.* **2019**, *100*, 035439.

(49) Kresse, G.; Hafner, J. Ab Initio Molecular-Dynamics Simulation of the Liquid-Metal− Amorphous-Semiconductor Transition in Germanium. *Phys. Rev. B: Condens. Matter Mater. Phys.* **1994**, *49*, 14251−14269.

(50) Kresse, G.; Hafner, J. Ab Initio Molecular Dynamics for Liquid Metals. *Phys. Rev. B: Condens. Matter Mater. Phys.* **1993**, *47*, 558−561.

(51) Kresse, G.; Furthmüller, J. Efficient Iterative Schemes for Ab Initio Total-Energy Calculations Using a Plane-Wave Basis Set. *Phys. Rev. B: Condens. Matter Mater. Phys.* **1996**, *54*, 11169−11186.

(52) Kresse, G.; Furthmüller, J. Efficiency of Ab-Initio Total Energy Calculations for Metals and Semiconductors Using a Plane-Wave Basis Set. *Comput. Mater. Sci.* **1996**, *6*, 15−50.

(53) Kresse, G.; Joubert, D. From Ultrasoft Pseudopotentials to the Projector Augmented-Wave Method. *Phys. Rev. B: Condens. Matter Mater. Phys.* **1999**, *59*, 1758−1775.

(54) Sun, J.; Xiao, B.; Ruzsinszky, A. Communication: Effect of the Orbital-Overlap Dependence in the Meta Generalized Gradient Approximation. *J. Chem. Phys.* **2012**, *137*, 051101.

(55) Sun, J.; Haunschild, R.; Xiao, B.; Bulik, I. W.; Scuseria, G. E.; Perdew, J. P. Semilocal and Hybrid Meta-Generalized Gradient Approximations Based on the Understanding of the Kinetic-Energy-Density Dependence. *J. Chem. Phys.* **2013**, *138*, 044113.

(56) Blöchl, P. E. Projector Augmented-Wave Method. *Phys. Rev. B: Condens. Matter Mater. Phys.* **1994**, *50*, 17953−17979.

(57) Maeland, A.; Flanagan, T. B. Lattice Spacings of Gold−Palladium Alloys. *Can. J. Phys.* **1964**, *42*, 2364−2366.

(58) Nichols, R. J.; Nouar, T.; Lucas, C. A.; Haiss, W.; Hofer, W. A. Surface Relaxation and Surface Stress of Au(111). *Surf. Sci.* **2002**, *513*, 263−271.

(59) Methfessel, M.; Paxton, A. T. High-Precision Sampling for Brillouin-Zone Integration in Metals. *Phys. Rev. B: Condens. Matter Mater. Phys.* **1989**, *40*, 3616−3621.

(60) Henkelman, G.; Jónsson, H. A Dimer Method for Finding Saddle Points on High Dimensional Potential Surfaces Using Only First Derivatives. *J. Chem. Phys.* **1999**, *111*, 7010−7022.

(61) Heyden, A.; Bell, A. T.; Keil, F. J. Efficient Methods for Finding Transition States in Chemical Reactions: Comparison of Improved Dimer Method and Partitioned Rational Function Optimization Method. *J. Chem. Phys.* **2005**, *123*, 224101.

(62) Kästner, J.; Sherwood, P. Superlinearly Converging Dimer Method for Transition State Search. *J. Chem. Phys.* **2008**, *128*, 014106.

(63) Xiao, P.; Sheppard, D.; Rogal, J.; Henkelman, G. Solid-State Dimer Method for Calculating Solid-Solid Phase Transitions. *J. Chem. Phys.* **2014**, *140*, 174104.

(64) Gerrits, N.; Migliorini, D.; Kroes, G.-J. Dissociation of CHD₃ on Cu(111), Cu(211), and Single Atom Alloys of Cu(111). *J. Chem. Phys.* **2018**, *149*, 224701.

(65) Plimpton, S. Fast Parallel Algorithms for Short-Range Molecular Dynamics. *J. Comput. Phys.* **1995**, *117*, 1−19.

(66) Singraber, A.; Behler, J.; Dellago, C. Library-Based LAMMPS Implementation of High-Dimensional Neural Network Potentials. *J. Chem. Theory Comput.* **2019**, *15*, 1827−1840.

(67) Behler, J.; Parrinello, M. Generalized Neural-Network Representation of High-Dimensional Potential-Energy Surfaces. *Phys. Rev. Lett.* **2007**, *98*, 146401.

(68) Behler, J. Representing Potential Energy Surfaces by High-Dimensional Neural Network Potentials. *J. Phys.: Condens. Matter* **2014**, *26*, 183001.

(69) Behler, J. Atom-Centered Symmetry Functions for Constructing High-Dimensional Neural Network Potentials. *J. Chem. Phys.* **2011**, *134*, 074106.

(70) Behler, J. Constructing High-Dimensional Neural Network Potentials: A Tutorial Review. *Int. J. Quantum Chem.* **2015**, *115*, 1032−1050.

(71) Behler, J. First Principles Neural Network Potentials for Reactive Simulations of Large Molecular and Condensed Systems. *Angew. Chem., Int. Ed.* **2017**, *56*, 12828−12840.

(72) Behler, J. *RuNNer - A Neural Network Code for High-Dimensional Neural Network Potential-Energy Surfaces*; Universität Göttingen. http://www.uni-goettingen.de/de/560580.html, 2018.

(73) Gastegger, M.; Schwiedrzik, L.; Bittermann, M.; Berzsenyi, F.; Marquetand, P. wACSF—Weighted Atom-Centered Symmetry Functions as Descriptors in Machine Learning Potentials. *J. Chem. Phys.* **2018**, *148*, 241709.

(74) Kastanas, G. N.; Koel, B. E. Interaction of Cl_2 with the Au(111) Surface in the Temperature Range of 120 to 1000 K. *Appl. Surf. Sci.* **1993**, *64*, 235−249.

(75) Spencer, N. D.; Lambert, R. M. Chlorine Chemisorption and Surface Chloride Formation on Au(111). *Surf. Sci.* **1981**, *107*, 237−248.

(76) Davis, L. E.; MacDonald, N. C.; Palmberg, P. W.; Riach, G. E.; Weber, R. E. *Handbook of Auger Electron Spectroscopy: A Reference Book of Standard Data for Identification and Interpretation of Auger Electron Spectroscopy Data*, 2nd ed.; Physical Electronics Industries: Eden Prairie, MN, 1976.

(77) Dion, M.; Rydberg, H.; Schröder, E.; Langreth, D. C.; Lundqvist, B. I. Van Der Waals Density Functional for General Geometries. *Phys. Rev. Lett.* **2004**, *92*, 246401.

(78) Jackson, B.; Nave, S. The Dissociative Chemisorption of Methane on Ni(111): The Effects of Molecular Vibration and Lattice Motion. *J. Chem. Phys.* **2013**, *138*, 174705.

(79) Guo, H.; Farjamnia, A.; Jackson, B. Effects of Lattice Motion on Dissociative Chemisorption: Toward a Rigorous Comparison of Theory with Molecular Beam Experiments. *J. Phys. Chem. Lett.* **2016**, *7*, 4576−4584.

(80) Polanyi, J. C. Concepts in Reaction Dynamics. *Acc. Chem. Res.* **1972**, *5*, 161−168.

(81) Marcus, R. A. On the Analytical Mechanics of Chemical Reactions. Quantum Mechanics of Linear Collisions. *J. Chem. Phys.* **1966**, *45*, 4493−4499.

(82) McCullough, E. A.; Wyatt, R. E. Quantum Dynamics of the Collinear (H, H_2) Reaction. *J. Chem. Phys.* **1969**, *51*, 1253−1254.

(83) Smith, R. R.; Killelea, D. R.; DelSesto, D. F.; Utz, A. L. Preference for Vibrational over Translational Energy in a Gas-Surface Reaction. *Science* **2004**, *304*, 992−995.

(84) Díaz, C.; Olsen, R. A. A Note on the Vibrational Efficacy in Molecule-Surface Reactions. *J. Chem. Phys.* **2009**, *130*, 094706.

(85) Head-Gordon, M.; Tully, J. C. Molecular Dynamics with Electronic Frictions. *J. Chem. Phys.* **1995**, *103*, 10137−10145.

(86) Askerka, M.; Maurer, R. J.; Batista, V. S.; Tully, J. C. Role of Tensorial Electronic Friction in Energy Transfer at Metal Surfaces. *Phys. Rev. Lett.* **2016**, *116*, 217601.

(87) Maurer, R. J.; Jiang, B.; Guo, H.; Tully, J. C. Mode Specific Electronic Friction in Dissociative Chemisorption on Metal Surfaces: H_2 on Ag(111). *Phys. Rev. Lett.* **2017**, *118*, 256001.

(88) Spiering, P.; Meyer, J. Testing Electronic Friction Models: Vibrational De-Excitation in Scattering of H_2 and D_2 from Cu(111). *J. Phys. Chem. Lett.* **2018**, *9*, 1803−1808.

(89) Goodman, F. O.; Wachman, H. Y. *Formula for Thermal Accommodation Coefficient* **1966**, AD0631007.

(90) Gerrits, N.; Chadwick, H.; Kroes, G.-J. Dynamical Study of the Dissociative Chemisorption of CHD_3 on Pd(111). *J. Phys. Chem. C* **2019**, *123*, 24013−24023.

(91) Gerrits, N.; Kroes, G.-J. An AIMD Study of Dissociative Chemisorption of Methanol on Cu(111) with Implications for Formaldehyde Formation. *J. Chem. Phys.* **2019**, *150*, 024706.

(92) Tully, J. C. Theories of the Dynamics of Inelastic and Reactive Processes at Surfaces. *Annu. Rev. Phys. Chem.* **1980**, *31*, 319−343.

(93) Zhou, X.; Jiang, B. A Modified Generalized Langevin Oscillator Model for Activated Gas-Surface Reactions. *J. Chem. Phys.* **2019**, *150*, 024704.

(94) Jackson, B.; Nattino, F.; Kroes, G.-J. Dissociative Chemisorption of Methane on Metal Surfaces: Tests of Dynamical Assumptions Using Quantum Models and Ab Initio Molecular Dynamics. *J. Chem. Phys.* **2014**, *141*, 054102.

(95) Migliorini, D.; Nattino, F.; Tiwari, A. K.; Kroes, G.-J. HOD on Ni(111): Ab Initio Molecular Dynamics Prediction of Molecular Beam Experiments. *J. Chem. Phys.* **2018**, *149*, 244706.

(96) Shenvi, N.; Roy, S.; Tully, J. C. Nonadiabatic Dynamics at Metal Surfaces: Independent-Electron Surface Hopping. *J. Chem. Phys.* **2009**, *130*, 174107.

(97) Cooper, R.; Bartels, C.; Kandratsenka, A.; Rahinov, I.; Shenvi, N.; Golibrzuch, K.; Li, Z.; Auerbach, D. J.; Tully, J. C.; Wodtke, A. M. Multiquantum Vibrational Excitation of NO Scattered from Au(111): Quantitative Comparison of Benchmark Data to Ab Initio Theories of Nonadiabatic Molecule−Surface Interactions. *Angew. Chem., Int. Ed.* **2012**, *51*, 4954−4958.

(98) Hanke, F.; Björk, J. Structure and Local Reactivity of the Au(111) Surface Reconstruction. *Phys. Rev. B: Condens. Matter Mater. Phys.* **2013**, *87*, 235422.

(99) Zhang, Y.; Hu, C.; Jiang, B. Embedded Atom Neural Network Potentials: Efficient and Accurate Machine Learning with a Physically Inspired Representation. *J. Phys. Chem. Lett.* **2019**, *10*, 4962−4967.

(100) Kumar, S.; Jiang, H.; Schwarzer, M.; Kandratsenka, A.; Schwarzer, D.; Wodtke, A. M. Vibrational Relaxation Lifetime of a Physisorbed Molecule at a Metal Surface. *Phys. Rev. Lett.* **2019**, *123*, 156101.

(101) Chadwick, H.; Migliorini, D.; Kroes, G. J. CHD_3 Dissociation on Pt(111): A Comparison of the Reaction Dynamics Based on the PBE Functional and on a Specific Reaction Parameter Functional. *J. Chem. Phys.* **2018**, *149*, 044701.

(102) Lee, K.; Murray, É. D.; Kong, L.; Lundqvist, B. I.; Langreth, D. C. Higher-Accuracy van Der Waals Density Functional. *Phys. Rev. B: Condens. Matter Mater. Phys.* **2010**, *82*, 081101.

(103) Migliorini, D.; Nattino, F.; Kroes, G.-J. Application of van Der Waals Functionals to the Calculation of Dissociative Adsorption of N2 on W(110) for Static and Dynamic Systems. *J. Chem. Phys.* **2016**, *144*, 084702.

(104) Behler, J.; Delley, B.; Lorenz, S.; Reuter, K.; Scheffler, M. Dissociation of O_2 at Al(111): The Role of Spin Selection Rules. *Phys. Rev. Lett.* **2005**, *94*, 036104.

(105) Livshits, E.; Baer, R.; Kosloff, R. Deleterious Effects of Long-Range Self-Repulsion on the Density Functional Description of O_2 Sticking on Aluminum. *J. Phys. Chem. A* **2009**, *113*, 7521−7527.

(106) See the SRS user manual for the IGC100 ion gauge controller for an overview of ion gauge accuracy and stability, available at their Web site under https://www.thinksrs.com/products/igc100.html